The Journal of Immunology

NLRP6 Deficiency in CD4 T Cells Decreases T Cell Survival Associated with Increased Cell Death

Katarina Radulovic, C. Korcan Ayata, Rachel Mak'Anyengo, Kristina Lechner, Philipp Wuggenig, Berna Kaya, Petr Hruz, Mercedes Gomez de Agüero, Petr Broz, Benno Weigmann and Jan Hendrik Niess

J Immunol published online 31 May 2019
http://www.jimmunol.org/content/early/2019/05/30/jimmunol.1800938

Supplementary Material **http://www.jimmunol.org/content/suppl/2019/05/31/jimmunol.1800938.DCSupplemental**

The Journal of Immunology is published twice each month by The American Association of Immunologists, Inc., 1451 Rockville Pike, Suite 650, Rockville, MD 20852

Print ISSN: 0022-1767 Online ISSN: 1550-6606.

Published May 31, 2019, doi:10.4049/jimmunol.1800938

NLRP6 Deficiency in CD4 T Cells Decreases T Cell Survival Associated with Increased Cell Death

Katarina Radulovic,*,†,[1] C. Korcan Ayata,*,[1] Rachel Mak'Anyengo,* Kristina Lechner,‡ Philipp Wuggenig,* Berna Kaya,* Petr Hruz,§ Mercedes Gomez de Agüero,¶ Petr Broz,‖ Benno Weigmann,‡ and Jan Hendrik Niess*,§

The nucleotide-binding oligomerization domain (NOD)-like receptors belong to the family of pattern recognition receptors (PRRs). NOD-like receptors play a role in regulation of innate immune response by recognition of both pathogen-associated molecular patterns that are engulfed during phagocytic process and danger-associated molecular patterns that are mainly byproducts of cell stress mediated response. NOD-like family pyrin domain containing 6 (NLRP6) is one of the 14 pyrin domain–containing receptors. NLRP6 is highly expressed by epithelial and goblet cells to regulate epithelial renewal and mucus production in mice and humans, but its function in T cells is rather unknown. Increased caspase-1 activation and cell death were observed in mouse *Nlrp6*–deficient T cells following adoptive transfer into *Rag2*-deficient mice, indicating that *Nlrp6* deficiency in CD4$^+$ T cells led to decreased survival. ***The Journal of Immunology*****, 2019, 203: 000–000.**

Nucleotide-binding oligomerization domain (NOD)-like family pyrin domain containing 6 (NLRP6) is a member of the NOD-like receptor (NLR) family (1, 2). NLRP6 may be involved in the assembly of the inflammasome leading to the posttranslational activation of IL-1β and IL-18 through caspase-1 (3). Caspase-1, together with caspase-11, can induce pyroptosis by activating gasdermin D, leading to the release of danger-associated molecular patterns in response to an infection to induce an innate immune response (4). NLRP6 can also inhibit the canonical NF-κB pathway to suppress the production of proinflammatory cytokines in infected macrophages (5). Furthermore, NLRP6 recognizes viral ssRNA. It has been shown that by binding to RNA helicase Dhx15 of encephalomyocarditis virus, NLRP6 induces the production of type I and III IFN and the transcription of IFN-stimulated genes (6). The microbial-derived metabolites taurine and spermidine have also been suggested as potential ligands of NLRP6 (7). Recently, lipoteichoic acid, a constituent of the cell wall of Gram-positive bacteria, has been identified as a ligand for NLRP6 (8). Hence, NLRP6 has an important function in regulating interactions between the host and the microbiota (8). Indeed, NLRP6 is highly abundant in the small and large intestine and is specifically expressed by intestinal epithelial cells (IECs) and goblet cells (9–11).

NLRP6 protects mice against dextran sulfate sodium–induced colitis and colitis-associated cancer (12, 13) and also protects IL-10–deficient animals against spontaneous colitis (14). This may be explained by impaired IL-18 production in *Nlrp6*-deficient animals (12). NLRP6 also regulates the release of mucus in sentinel goblet cells after invasion of microorganism into the inner mucus layer; therefore, the release of mucus is impaired in *Nlrp6*-deficient animals, resulting in goblet cell hyperplasia (10, 11). Furthermore, microbial colonization is regulated through NLRP6 by secretion of antimicrobial peptides (7). Consequently, *Nlrp6*-deficient mice have a dysbiotic microbiota in which *Prevotella* and *Candidatus Saccharibacteria* species are enriched (7, 12), which can be transferred to wild-type (wt) animals by cohousing. However, in different animal facilities, variants in the composition of the microbiota between wt and *Nlrp6*-deficient mice is explained by cage effects and mother variates, but not by genotype (15). Usage of littermates shows that sex of the mice, but not *Nlrp6* deficiency, influences the composition of the microbiota (16). Therefore, susceptibility to dextran sulfate sodium–induced colitis is comparable between wt and Nlrp6-deficient littermate mice (15, 16). Perhaps, this discrepancy may be explained by the microbiota transmitted to wt or *Nlrp6*-deficient mice (17). The transmission of a pathobiont-free microbiota did not result in variants of the microbiota in wt and *Nlrp6*-deficient mice, whereas the transmission of a microbiota containing pathobionts resulted into dysbiosis in *Nlrp6*-deficient, but not in wt, mice (17).

Although IECs highly express NLRP6, the reconstitution of lethally irradiated wt animals with *Nlrp6*-deficient bone marrow (BM) leads to

*Department of Biomedicine, University of Basel, CH-4031 Basel, Switzerland; †Unité de Recherche Clinique, Centre Hospitalier de Valenciennes, 59322 Valenciennes, France; ‡Department of Medicine I, University Medical Center, 91054 Erlangen, Germany; §University Center for Gastrointestinal and Liver Diseases, St. Clara Hospital and University Hospital, CH-4031 Basel, Switzerland; ¶Department of Biomedical Research, Maurice Müller Laboratories, University of Bern, CH-3008 Bern, Switzerland; and ‖Department of Biochemistry, University of Lausanne, 1066 Epalinges, Switzerland

[1]K.R. and C.K.A. contributed equally to this work.

ORCIDs: 0000-0003-1003-2500 (K.R.); 0000-0003-3184-2799 (K.L.); 0000-0003-2301-7772 (P.W.); 0000-0002-7132-290X (M.G.d.A.); 0000-0002-2398-0844 (B.W.); 0000-0001-6902-5650 (J.H.N.).

Received for publication July 6, 2018. Accepted for publication May 7, 2019.

This work was supported by Swiss National Science Foundation Grant 310030_175548 and the United European Gastroenterology (UEG) Week top abstract prize (to J.H.N.) awarded at the UEG Week, October 19 to 23, 2018, in Vienna, Austria.

The sequences presented in this article have been submitted to the Gene Expression Omnibus under accession number GSE116454.

Address correspondence and reprint requests to Dr. Jan Hendrik Niess, University Center for Gastrointestinal and Liver Diseases, St. Clara Hospital and University Hospital, Basel, Switzerland, Petersgraben 4, CH-4031 Basel, Switzerland. E-mail address: janhendrik.niess@usb.ch

The online version of this article contains supplemental material.

Abbreviations used in this article: BM, bone marrow; BMDC, BM-derived DC; BMDM, BM-derived macrophage; cLP, colonic lamina propria; DC, dendritic cell; DPBS-Prep, Dulbecco's PBS preparation; GF, germ-free; IEC, intestinal epithelial cell; mln, mesenteric lymph node; NLR, NOD-like receptor; NLRP6, NOD-like family pyrin domain containing 6; NOD, nucleotide-binding oligomerization domain; PS, phosphatidylserine; qPCR, quantitative PCR; RNA-seq, RNA sequencing; siLP, small intestine lamina propria; SPF, specific pathogen-free; Treg, FOXP3-positive regulatory T; wt, wild-type.

similar colitis-associated tumor formation as in *Nlrp6*-deficient animals (9). Conversely, the reconstitution of lethally irradiated *Nlrp6*-deficient animals with wt BM leads to reduced tumor formation compared with *Nlrp6*-deficient animals. This indicates that hematopoietic, rather than epithelial cells, are required for the differential regulation of colitis-associated tumor development between wt and *Nlrp6*-deficient mice (9). Nevertheless, physiologically relevant function of NLRP6 in most hematopoietic cells has not been investigated.

In this study, we show that Th1 cells express NLRP6 after differentiation from naive T cells. By using in vitro assays and cotransfer experiments of wt and *Nlrp6*-deficient T cells in *Rag2*-deficient hosts, the potential influence of NLRP6 on the microbiota and the influence of the microbiota on T cells in mice with different genotypes have been minimized. *Nlrp6*-deficient T cells produced less IFN-γ in vitro, and increased frequencies of dead T cells were observed after transfer of *Nlrp6*-deficient T cells in *Rag2*-deficient hosts. Therefore, this study provides, to our knowledge, a novel mechanism revealing a physiological role of NLRP6 in T cells that is independent of potential variances in the composition of the microbiota in wt and *Nlrp6*-deficient mice.

Materials and Methods

Mice

C57BL/6, *Nlrp6*$^{-/-}$, *Cd45.1* (Ly-5.1; B6.SJL-Ptprc$^{Pepc/BoyJ}$), Tbx21$^{tm1/Glm}$, *Asc*$^{-/-}$, and *Rag2*$^{-/-}$ mice were kept under specific pathogen-free (SPF) conditions in the animal colonies of the Department of Biomedicine, University of Basel (Basel, Switzerland); the Center of Molecular Sciences, University of Basel; or the University Medical Center, University of Erlangen, (Erlangen, Germany). Germ-free (GF) C57BL/6 mice were kept at the clean mouse facility at the University of Bern, Switzerland. Millennium Pharmaceuticals originally generated *Nlrp6*$^{-/-}$ mice, and the Takeda Oncology company agreed that *Nlrp6*$^{-/-}$ mice could be used in our studies (study no PCRS-2016-101530). Six- to twelve-week-old animals were used for experiments. All animal experiments were conducted in accordance to the Swiss Federal and Cantonal regulations, and the animal protocol approved by the local animal welfare committee (animal protocol no. 2871 [Canton of Basel-Stadt]).

CD45RB^{high} CD4 T cell transfer colitis and cotransfer experiments

Splenocytes were isolated from *Nlrp6*$^{-/-}$ or *Cd45.1*$^{+/-}$ C57BL/6 or *wt* C57BL/6 mice. CD19$^+$ B cells and CD8$^+$ T cells were magnetically depleted by positive selection (MojoSort, BioLegend). Supernatants containing CD4$^+$ T cells were collected, washed, and counted. Fixable viability dye eFluor 450 (eBioscience) was added to the cells. Cells were then stained with anti-mouse CD3e AF700 (BioLegend), anti-mouse CD4 BV510 (BioLegend), and anti-mouse CD45RB FITC (BioLegend) Abs, viable naive CD3$^+$CD4$^+$CD45RB^{high} cells were sorted with either BD FACSAria III or BD Influx cell sorters. A total of 3×10^5 naive CD3$^+$CD4$^+$CD45RB^{high} cells were injected intraperitoneally into *Rag2*$^{-/-}$ host. In cotransfer experiments, equal numbers (1.5×10^5) of wt (*Cd45.1*) and *Nlrp6*$^{-/-}$ (*Cd45.2*) CD4$^+$CD45RB^{high} T cells were injected intraperitoneally into *Rag2*$^{-/-}$ mice. Disease scores were assessed as follows: rectal bleeding, 0 indicates absence and 1 indicates bleeding; rectal prolapse, 0 indicates absence and 6 indicates prolapse; stool consistency, 0 indicates absence, 1 indicates loose stools, and 2 indicates diarrhea; position, 0 indicates normal movements, 1 indicates reluctance to move, and 2 indicates hunched position; fur, 0 indicates normal appearance, 1 indicates ruffled fur, and 2 indicates spiky fur; and weight loss, 0 indicates no body weight loss, 1 indicates body weight loss 0–5%, 2 indicates body weight loss >5–10%, 3 indicates body weight loss >10–15%, and 4 indicates body weight loss >15%. The animals were monitored twice a week, and when a score ≥4 occurred, the animals were monitored twice a day. Experiment had to be stopped when a total score ≥6, when an individual animals loose >15% body weight, or when gross bleeding or rectal prolapses were observed. At indicated time points, CD4 T cells were isolated from the indicated organs and further analyzed by flow cytometry.

Intestinal lamina propria and epithelial cell isolation

Tissue from the small and large intestine were collected, Peyer patches were removed, and small intestine was cut in five to six pieces. Samples were washed with PBS to remove debris and mucous, and the epithelium was removed by incubation in 5 mM EDTA in Ca^{2+}/Mg^{2+}-free PBS at 37°C under gentle shaking for 3×10 min. Between the incubation steps, the tubes were vortexed for 30 s. Supernatants were collected after each incubation, from which cells were pelleted and the epithelial cells were enriched using the Percoll gradient. In 15-ml tube, 40% Percoll in PBS was carefully pipetted under the layer of 20% Percoll in RPMI; then, the pelleted cells were diluted in RPMI and overlaid on the top of the 20% Percoll layer. This gradient was centrifuged at $600 \times g$ for 30 min, and epithelial cells were collected between 20% Percoll and upper RPMI phase. Cells were washed with PBS before further usage for RNA extraction. The remaining tissue fragments were washed in PBS and cut as small as possible with a pair of scissors. The tissue was digested with 0.5 mg/ml collagenase type VIII (Sigma-Aldrich) and 10 U/ml DNase I (Roche) in RPMI 1640 for 20–25 min at 37°C in a water bath with continuous shaking (200 rpm). Every 5 min, the tubes were vortexed for 30 s. Supernatants were collected, passed through a 70-μm cell strainer, and lamina propria cells were pelleted and counted.

Cell isolation from mesenteric lymph nodes, thymus, and spleen

Single-cell suspensions from mesenteric lymph nodes (mln), thymus, and spleens were prepared by mashing the tissue through 70-μm cell strainer; RBC in spleen were lysed with ammonium chloride Tris buffer (144 mM NH_4Cl and 17 mM Tris; pH 7.2). After the lysis, cells were washed, counted, and used for flow cytometry, in vitro, or in vivo experiments.

BM-derived macrophages and dendritic cells

For the preparation, femurs and tibias of hind legs were used, and BM was flushed out using a syringe and a 25-gauge needle. BM cells were collected and passed through a 70-μm cell strainer to remove bone spicules and cell clumps. RBC were lysed with ammonium chloride Tris buffer (144 mM NH_4Cl and 17 mM Tris; pH 7.2). The cells were then cultured in six-well plates with plating concentration 4×10^6 cells/well. Macrophages were differentiated in RPMI 1640 medium (Life Technologies) containing 10% FCS, 0.05 mM 2-ME, 100 U/ml penicillin, and 100 μg/ml streptomycin in presence of 20 ng/ml M-CSF (BioLegend). Culturing medium for macrophages were changed on days 3 and 5 of culture, and mature macrophages were collected as adherent cells after 7 d of culture. Dendritic cells (DCs) were generated in IMDM (Life Technologies) supplemented with 10% FCS, 0.05 mM 2-ME, 100 U/ml penicillin, and 100 μg/ml streptomycin in presence of 100 ng/ml human FLT3L (kindly provided by R. Tussiwand). Mature DCs were collected after 10–12 d of culture without any medium change. The viability and purity of macrophages and DCs were confirmed with flow cytometry.

Neutrophil isolation from BM

After flushing out BM cells from femurs and tibias of hind legs with Dulbecco's PBS preparation (DPBS-Prep; PBS, 20 mM HEPES, and 0.5% [v/v] FCS) cells were passed through 70-μm cell strainer and pelleted. For RBC lysis, cells were resuspended in 10 ml 0.2% NaCl for 30 s and 10 ml 1.6% NaCl was added to stop the lysis. Cells were resuspended in 5 ml DPBS-Prep, overlaid on 62.5% Percoll, and centrifuged at $1000 \times g$ for 30 min with brake 3 on acceleration and no deceleration brake. The upper medium was removed carefully, and the cloudy pellet at the bottom containing the neutrophils was washed with DPBS-Prep and further processed for RNA isolation.

T cell differentiation assay

Naive CD4 T cells were purified from spleens of C57BL/6, *Nlrp6*$^{-/-}$, *Asc*$^{-/-}$, or *Tbx21*$^{-/-}$ mice with a naive CD4 T Cell Isolation Kit (BioLegend) and resuspended in IMDM medium containing 10% FCS and supplemented with 50 μM 2-ME, 100 U/ml penicillin, and 100 μg/ml streptomycin. Naive CD4 T cells (5.0×10^4 cells per well) were placed in 96-well, flat-bottom plates, which had been coated with 5 μg/ml anti-CD3 Ab 145-2C11 (BioLegend). A total of 5 μg/ml soluble anti-CD28 37.51 Ab (eBioscience) was added to all wells. Th1 cells were differentiated in the presence of 10 μg/ml anti–IL-4 11B11 Ab (BioLegend), 20 ng/ml IL-2 (R&D Systems), and 20 ng/ml IL-12 (R&D Systems). Th2 cells were differentiated in the presence of 10 μg/ml anti–IFN-γ XMG1.2 Ab (BioLegend), 20 ng/ml IL-2 (R&D Systems), and 20 ng/ml IL-4 (BioLegend). Th17 cells were generated in the presence of 10 μg/ml anti–IL-4 Ab, 10 μg/ml anti–IFN-γ Ab, 1 ng/ml hTGF-β (R&D Systems), 10 ng/ml IL-1β (R&D Systems), 50 ng/ml IL-6 (R&D Systems), and 20 ng/ml IL-23 (R&D Systems). FOXP3-positive regulatory T (Treg) cells were differentiated in the presence of 10 μg/ml anti–IL-4 Ab, 10 μg/ml anti–IFN-γ

Ab, 20 ng/ml IL-2 (R&D Systems), and 5 ng/ml hTGF-β (R&D Systems). Th1 and Th2 cells were transferred on the new noncoated plate at day 3 of culture when fresh medium containing only the differentiation cytokines was added to the cultures. Cells were harvested at indicated time points during 5 d of differentiation culture and analyzed for cell type specific markers by flow cytometry or lysed for RNA isolation for quantitative PCR (qPCR).

Surface marker staining for flow cytometry

Isolated cells were washed in PBS, counted, and stained with fixable viability dye eFluor 455UV or eFluor 450 (eBioscience), together with mAb 2.4G2 (eBioscience), directed against the FcγRIII/II CD16/CD32 (0.5 mg mAb/1 × 10^6 cells) to prevent nonspecific binding of Abs to Fc receptors in PBS for 30 min at 4˚C. Cells were then washed in PBS/2% FBS supplemented with 0.1% w/v sodium azide and 10 mM EDTA, incubated with the relevant mAb for 20 min at 4˚C, and washed again twice. When biotin-coupled primary Abs were used, cells were incubated with streptavidin/eFluor 450 (eBioscience) or streptavidin/PE/Cy5 (BioLegend) for 20 min at 4˚C. Data were acquired with Fortessa flow cytometers (BD Biosciences) and analyzed using FlowJo software version 10.0.7r2 (Tree Star). In all experiments, forward scatter height versus forward scatter area was used to gate on singlets, whereas dead cells were excluded using the fluorescence-coupled fixable viability dye.

The following mAbs were used for surface staining: anti-CD3/AF700 17A2 (BioLegend), anti-CD4/BV510 RM4-5 (BioLegend), anti–CD8a/FITC 53-6.7 (BioLegend), anti-CD45RB/FITC C363-16A (BioLegend), anti-CD45/eVolve655 30-F11 (eBioscience), anti-TCRβ/PE H57-597 (eBioscience), anti-CD45.2/biotin 104 (BioLegend), anti-CD8a/biotin 53-6.7 (BioLegend), and anti-CD19/biotin 6D5 (BioLegend).

Intracellular cytokine staining

T cells from cultures or cells isolated from indicated organs were stimulated for 4 h at 37˚C with 50 ng/ml PMA (Sigma-Aldrich) and 750 ng/ml ionomycin (Sigma-Aldrich) in the presence of 3 μg/ml brefeldin A (eBioscience). The cells were then washed and stained with fixable viability dye eFluor 455UV (eBioscience). Surface staining with anti-CD45 and CD4 T cell Abs was done before fixation and permeabilization (Fixation/Permeabilization Buffer; BD Biosciences). Permeabilized cells were incubated for 30 min at 4˚C in the dark with the following Abs: anti–IFN-γ/FITC XMG1.2 (BD Biosciences), anti–IL-17A/PE/Cy7 eBio17B7 (eBioscience), anti–IL-13/PE eBio13A (eBioscience), and anti–IL-10/PE JES5-16E3 (eBioscience). Stained cells were washed twice in permeabilization buffer and once with PBS supplemented with 2% FCS and 0.1% w/v sodium azide and 10 mM EDTA before flow cytometry.

Intracellular Foxp3 staining

Foxp3/Transcription Factor Staining Buffer Set (eBioscience) was used to determine the nuclear expression of FOXP3 after in vitro differentiation into Treg cells. Cells were first stained with fixable viability dye eFluor 450, after which, the fixation/permeabilization solution was applied. After overnight incubation on 4˚C in the dark, cells were pelleted and washed twice with 1× Permeabilization Buffer. Anti-Foxp3/AF647 150D (BioLegend) Ab was applied in 1× Permeabilization Buffer, and cells were incubated for 30 min at room temperature in the dark. After two times washing, cells were analyzed by BD Fortessa.

CFSE cell proliferation and Ki67 staining

Proliferation of cells was determined with CellTrace CFSE Cell Proliferation Kit for Flow Cytometry (no. C34570; Thermo Fisher Scientific). Briefly, 1–10 × 10^6 cells/ml in PBS and 0.1% BSA were incubated at 37˚C for 10 min in a CFSE final concentration of 1 μM, washed two times in 20 ml IMDM/10% FCS medium, and placed in cultures under Th1-polarizing conditions. Cells were collected from culture at indicated time points, stained with fixable viability dye eFluor 455UV, and analyzed by flow cytometry.

For the Ki67 staining, T cells were collected at indicated time points, washed, pelleted, and stained with fixable viability dye eFluor 450. Three milliliters of ice-cold 70% ethanol was added to each sample drop by drop while the tube with the cells was vortexed in the same time. Vortex was continued for 30 s after adding all the ethanol, and the samples were incubated in 70% ethanol for 1 h at −20˚C. T cells were then pelleted, washed twice, and incubated with anti-mouse Ki67/APC 16A8 (BioLegend) Ab for 30 min at room temperature in the dark, washed, and analyzed by flow cytometry.

Western blot and apoptosis signaling pathway array

In vitro–differentiated wt and *Nlrp6*-deficient Th1 cells were homogenized with ice-cold radioimmunoprecipitation buffer containing complete protease/phosphatase inhibitor mixture (Santa Cruz Biotechnology). Lysates were centrifuged at 18,000 × *g* at 4˚C for 20 min to remove cell debris. Bicinchoninic acid assay was performed for protein quantification. For Western blot, 20 μg protein was loaded in Mini-PROTEAN TGX 4–15% precast gels (Bio-Rad Laboratories) and transferred to nitrocellulose membrane using Trans-Blot Turbo (Bio-Rad Laboratories). The membrane was blocked with Odyssey Blocking Buffer TBS (LI-COR) for 1 h at room temperature and incubated with an anti–Caspase-1 Ab 5B10 (1:1000; Invitrogen) overnight at 4˚C. Biotin-conjugated donkey anti-rat Fab (1:10.000; Jackson ImmunoResearch Laboratories) and streptavidin conjugated IRDye 800CW (1:1000; LI-COR) were used for detection. Mouse anti-actin Ab-5 (1:1000; BD Biosciences) signal served as loading control. A mouse apoptosis signaling pathway array (AAM-APOSIG-1-4; RayBiotech) was used to compare wt and *Nlrp6*-deficient Th1 cells using manufacturers protocol. One hundred and fifty micrograms of protein was loaded to array membranes, primary Ab mixture incubation was overnight at 4˚C, biotinylated donkey anti-rabbit Fab (1:5.000; Jackson ImmunoResearch Laboratories) and streptavidin-conjugated IRDye 800CW (1:1000; LI-COR) were used for detection. Western blot and apoptosis array visualization were performed with Odyssey CLx (LI-COR), and the densitometric analysis was done using Image Studio Lite software v5.2.5 (LI-COR). Internal positive and negative controls were used for array normalization and background noise compensation.

Annexin V detection

An anti-mouse Annexin V Detection Kit (no. 88-8103-74; eBioscience) was used to stain phosphatidylserine (PS), which is located in the inner (cytoplasmic) layer of the cell membrane, thereby preventing binding of annexin V in intact cells. Pyroptotic cells form pores that allow the entrance of the annexin V Ab into the cells to stain PS in the cytoplasmic leaflet of the cell membrane. In apoptotic cells, PS moves from the inner to the outer layer of the cell membrane, where annexin V Ab binds, suggesting that both apoptotic and pyroptotic cells stain positive for annexin V (18, 19). After harvesting cells from indicated organs, cells were washed with PBS and stained with fixable viability dye eFluor 455UV. After washing with PBS/2% FCS, cells were stained for surface markers (CD45, TCRβ, and CD45.2). Cells were than washed with annexin V binding buffer and stained with annexin V/PE/Cy7 for 15 min at room temperature in the dark. Cells were washed, resuspended in annexin V binding buffer, and immediately analyzed by flow cytometry.

ELISA

Cell culture supernatants of 5-d differentiated wt and *Nlrp6*-deficient Th1 cells were collected and diluted 1:20. Mouse IFN-γ ELISA MAX kit (BioLegend) and Mouse IL-18 BPd DuoSet ELISA (R&D Systems) was used; standard curve and concentration calculations were done according to manufacturer's protocol.

Quantitative real time PCR

RNA was isolated from T and B cells sorted from spleens of C57BL/6 mice by lysis with TRI Reagent (Zymo Research) and using the Direct Zoll Mini Kit (Zymo Research) according to the manufacturer's protocol. In column, DNA digestion was performed as provided by the kit. RNA from BM-derived DCs (BMDCs), naive T cells, and in vitro–differentiated Th0, Th1, Th2, and Th17 cells was isolated by PureLink RNA Micro Scale Kit (Ambion), and DNA was also digested in column. IECs, BM-derived macrophages (BMDM), and neutrophils were lysed in TRI Reagent (Zymo Research), and RNA was isolated following the TRIzol Reagent User Guide (Invitrogen). From these samples, genomic DNA was removed using the TURBO DNA-free Kit (Ambion). RNA was reverse transcribed into cDNA using High-Capacity cDNA Reverse Transcription Kit (Invitrogen). The QuantiNova SYBR Green qPCR Kit (Qiagen) in 384-well plates, using gene specific primers to amplify genes of interest, and the reaction was analyzed on an Applied Biosystems Viia 7 cycler and software. All reactions were run in triplicates. Samples were normalized to the expression of actin-β (*Actb*) by calculating $2^{\delta Ct}$. Sequences of primers used in this study are presented in Table I.

RNA sequencing

Three weeks after the cell cotransfer into *Rag2*$^{-/-}$ hosts, wt CD4 T cells (live CD45$^+$TCRβ$^+$CD45.2$^-$ cells) and *Nlrp6*$^{-/-}$ CD4 T cells (live CD45$^+$TCRβ$^+$CD45.2$^+$ cells) were sorted by FACSAria III and lysed with TRI Reagent. RNA from these cells were isolated using PureLink RNA Micro Scale Kit (Ambion), and in column DNase treatment was done to digest genomic DNA. RNA quantification was made with NanoDrop ND-1000 Spectrophotometer (NanoDrop Technologies). Agilent Bioanalyzer

Table I. Primers used in the study

Primer	Sequence	Tm	Product Size (bp)
Nlrp6-F	5′-CAGACGCTGTGGACCTTGT-3′	59.5	199
Nlrp6-R	5′-ACGTGCTCGCGGTACTTCTT-3′	60.5	
Tbx21-F	5′-CAACCAGCACCAGACAGAGA-3′	60.5	111
Tbx21-R	5′-ACAAACATCCTGTAATGGCTTG-3′	58.4	
Gata3-F	5′-GCCTGCGGACTCTACCATAA-3′	60.5	94
Gata3-R	5′-AGGATGTCCCTGCTCTCCTT-3′	60.5	
Rorc-F	5′-CTGCAAAGAAGACCCACACC-3′	60.5	92
Rorc-R	5′-GGTGATAACCCCGTAGTGGA-3′	60.5	
Actb-F	5′-TTCTTTGCAGCTCCTTCGTT-3′	56.4	149
Actb-R	5′-ATGGAGGGGAATACAGCCC-3′	59.5	

Tm, melting temperature.

2100 instrument and RNA 6000 Nano Chip (Agilent Technologies) were used to assess the quality of RNA. The library was prepared with 220 ng total RNA using the TruSeq Stranded mRNA LT Sample Prep Kit (Illumina). Libraries were quality checked with the Fragment Analyzer (Advanced Analytical, Ames, IA) using the Standard Sensitivity NGS Fragment Analysis Kit (Advanced Analytical), revealing excellent quality of libraries (average concentration was 126 ± 13 nmol/l, and average library size was 345 ± 7 bp). After pooling of samples to equal molarity, each pool was quantified by PicoGreen Fluorometric measurement to be adjusted to 1.5 pM and used for clustering on the NextSeq 500 instrument (Illumina).

Samples were sequenced to produce single-end reads of 81 bases. Reads were aligned to the mouse genome (mm10) using the spliced read aligner STAR version 2.5.2a_modified (20). Default parameters were used, except for reporting only one location for multimappers in the final alignment files (outSAMmultNmax = 1) and filtering reads without evidence in the spliced junction table (outFilterType = "BySJout"). Sequencing and mapping quality was assessed by the qQCReport function of the R Bioconductor package QuasR version 1.18 (21). Gene expression was quantified by the qCount function of QuasR, as the number of reads that started within any annotated exon of a gene from the University of California, Santa Cruz Known Genes annotation (downloaded on 2015-12-18). The R Bioconductor package edgeR (version 3.20) was used for differential gene expression analysis (22). Between samples normalization was done using the trimmed mean of M-values normalization method method (23). After normalization, only genes with counts per million reads mapped values more than 1 in at least four samples were retained. An additive generalized linear model including the factor genotype (*Nlrp6*-deficient T cells and wt T cells) and controlling for differences across host mice (1–4) was fitted to the raw counts (function glmFit). Differential expression between *Nlrp6*-deficient T cells and wt T cells was evaluated by likelihood ratio tests (function glmLRT). The p values were adjusted by controlling the false discovery rate (FDR; Benjamini–Hochberg method), and genes with a FDR lower than 5% were considered differentially expressed. Gene set enrichment analysis was performed with the function camera from the edgeR package (using the default value of 0.01 for correlation of genes within gene sets) (24) and with all gene sets from the Molecular Signature Database (MSigDB v6.0) (25). We considered only sets from the hallmark collection (26) and containing more than 10 genes. We also built a manually curated list of gene sets for GSEA ("caspase," "cytochromes," "fadd," "granzyme," "interferon," "interleukin," "nlr," "ripk," "toll," and "traf"). Gene sets were considered enriched if they reached a FDR lower than 10%.

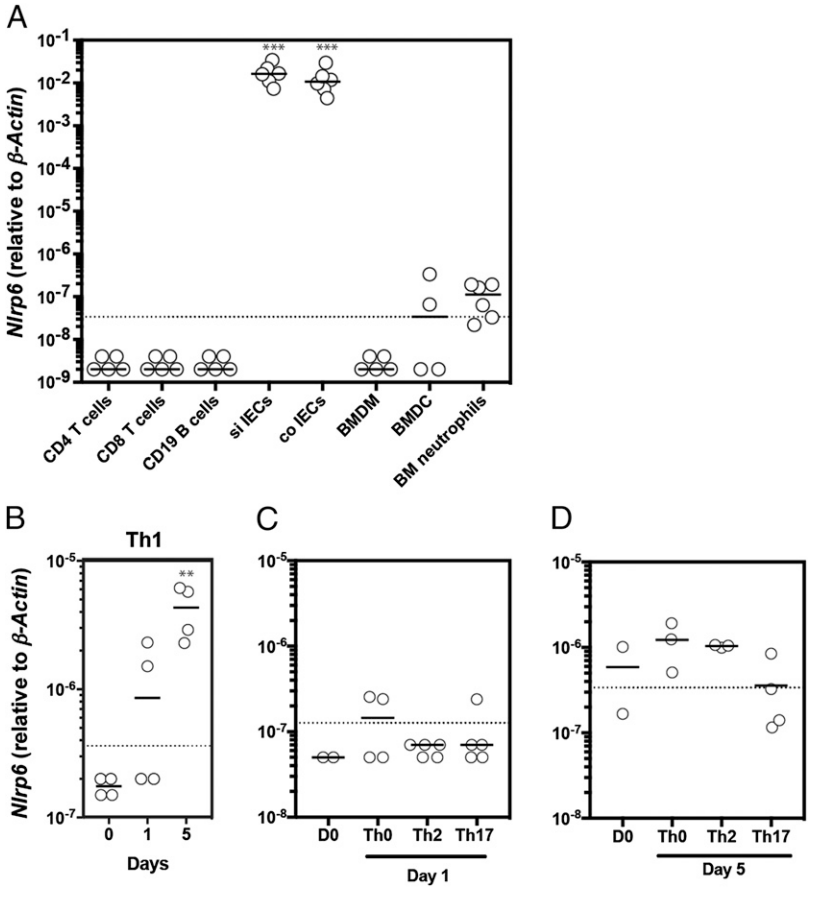

FIGURE 1. *Nlrp6* is expressed by Th1 cells. (**A**) $CD4^+$ T cells, $CD8^+$ T cells, and $CD19^+$ B cells were isolated from the spleen of C57BL/6 wt mice, small IECs (siIECs) and colonic epithelial cells (coIECs), and BM were isolated from the same animals. BMDM and BMDC were generated with M-CSF and FLT3L respectively, whereas neutrophils were directly isolated from the BM. *Nlrp6* expression was determined by qPCR. (**B**) Naive $CD4^+$ T cells were differentiated into Th1 cells, and *Nlrp6* expression was quantified by qPCR on days 1 and 5 of differentiation. Naive $CD4^+$ T cells (D0) were cultured in medium (Th0) or differentiated into Th2 or into Th17 cells for 1 d (**C**) or for 5 d (**D**) and used for *Nlrp6* expression analysis. Presented results are median of four to six samples; each dot represents one animal. The dotted line indicates the detection limit. The data were analyzed by Mann–Whitney U test. $^{**}p < 0.01$, $^{***}p < 0.001$.

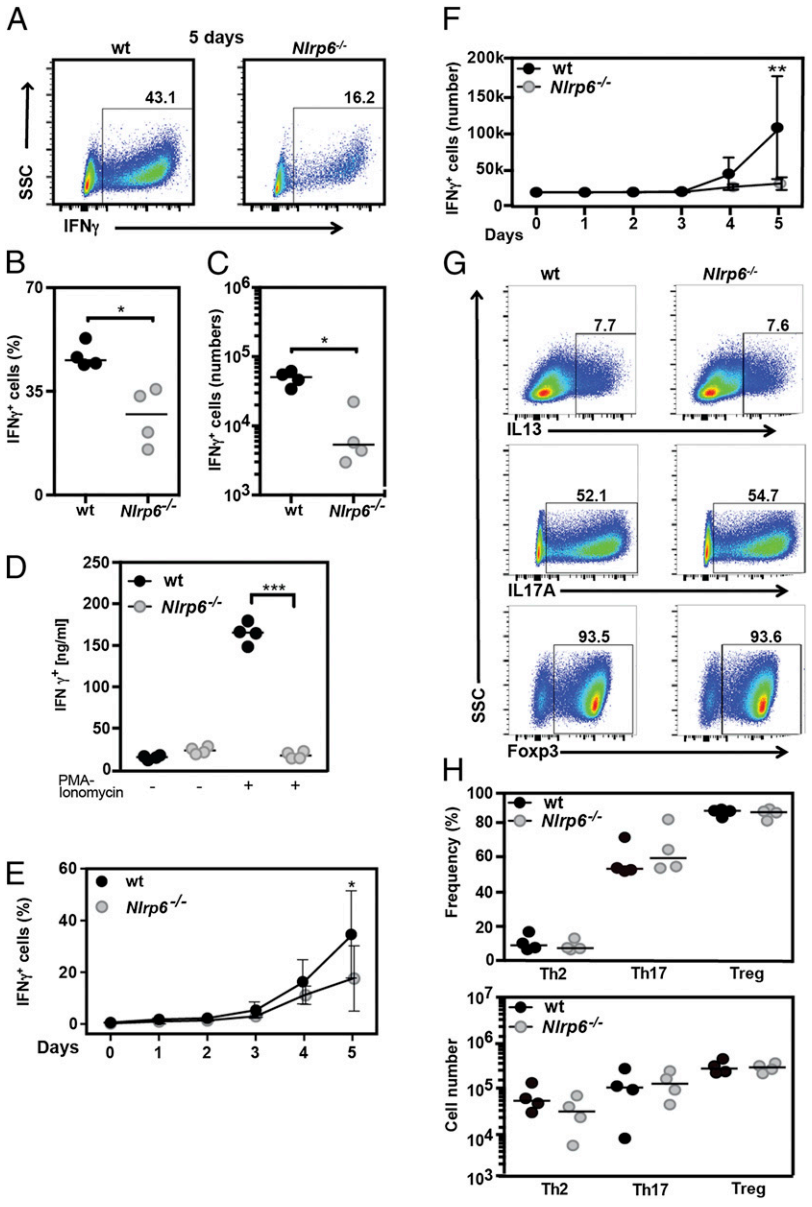

FIGURE 2. Reduced IFN-γ by *Nlrp6*-deficient Th1 cells. (**A**) Naive CD4$^+$ T cells from wt or *Nlrp6*-deficient mice were differentiated into Th1 cells, and IFN-γ–producing cells were measured by flow cytometry on day 5. (**B**) The percentage and (**C**) numbers of IFN-γ–producing wt and *Nlrp6*-deficient Th1 cells. Each data point represents one animal and the median is shown. The Mann–Whitney *U* test was used for data analysis. (**D**) IFN-γ production was quantified by ELISA in wt and *Nlrp6*-deficient Th1 cells before and after PMA/ionomycin stimulation. Naive CD4$^+$ T cells from wt (n = 3) or *Nlrp6*-deficient mice (n = 3) were differentiated for 5 d into Th1 cells. IFN-γ–producing cells were determined every single day by flow cytometry. (**E**) Percentage and (**F**) numbers of IFN-γ–producing T cells are presented. Data are mean and error bars represent SD. (**G**) Wt and *Nlrp6*-deficient naive CD4$^+$ T cells were differentiated into Th2 cells for 5 d and into Th17 cells and Foxp3$^+$ Treg cells for 4 d. IL-13– and IL-17A–producing cells following PMA/ionomycin stimulation and intracellular Foxp3$^+$ were determined by flow cytometry. Respective dot plots were obtained after gating on viable single cells. Percentages of IL-13$^+$, IL-17A$^+$, or Foxp3$^+$ T cells were indicated on respective gates. (**H**) Percentage and number of Th2, Th17, or Treg cells are presented. Each data point indicates an individual animal; results are shown as medians (n = 4 for each group). Data were analyzed with a Kruskal–Wallis test. $*p < 0.05$, $**p < 0.01$, $***p < 0.001$.

Statistics

For data analysis, GraphPad Prism software (version 7.0b) was used. Data were presented in scatter plots of individual samples with the median of each experimental group. Statistical significance was calculated with Mann–Whitney *U* test for two groups, or with Kruskal–Wallis test followed by Dunn correction for multiple comparisons. The p values are indicated as follows: $*p \leq 0.05$, $**p \leq 0.01$, and $***p \leq 0.001$.

Results

Nlrp6 is expressed by Th1 cells

Recent reports have suggested that NLRP6 is mainly expressed by IECs (10), but there are some indications that cells derived from the hematopoietic system may also express NLRP6 (9). The expression of *Nlrp6* was analyzed in CD4 and CD8 T cells, CD19 B cells, IECs isolated from the small and large intestine, M-CSF–differentiated BMDMs, FLT3L-differentiated BMDCs, and neutrophils isolated from the BM (Fig. 1A). Highest *Nlrp6* expression was observed in epithelial cells, confirming previous reports. Low expression level was observed in BMDCs and neutrophils isolated from the BM, whereas *Nlrp6* expression could not be detected in CD4$^+$ and CD8$^+$ T cells, CD19$^+$ B cells and BMDMs (Fig. 1A).

Next, naive CD4$^+$ T cells isolated from wt spleen were differentiated into Th1, Th2, and Th17 cells and analyzed for *Nlrp6* expression. We observed gradual increase in *Nlrp6* expression during 5 d of naive T cells culture under Th1 differentiation conditions. After 5 d of culture, expression was further upregulated (Fig. 1B). Th2 cells did not express *Nlrp6*, whereas only one out of five Th17 cell replicates expressed *Nlrp6* after 1 d of culture (Fig. 1C). Both Th2 and Th17 cells expressed *Nlrp6* after 5 d of culture. However, expression levels in Th2 and Th17 cells were lower compared with Th1 cells (Fig. 1D). *Tbx21*, *Gata3*, and *Rorc* expression confirmed the differentiation of naive T cells into Th1, Th2, and Th17, respectively (Supplemental Fig. 1). The analysis of genomic regions 1000 bp upstream of the starting site of human and mouse *Nlrp6* with the MatInspector software (Genomatix) revealed binding sites for STAT1, STAT5a, and TBX21, whereas EOMES binding sites could only be found upstream of human *NLRP6* (Supplemental Fig. 2A, 2B). Consequently, to validate TBX21 binding site, *Nlrp6* expression analysis was performed in *Tbx21*-deficient T cells cultured in Th1-differentiation conditions. *Nlrp6* was not expressed in *Tbx21*-deficient T cells cultured for 2 d under Th1-polarizing conditions (Supplemental Fig. 2C).

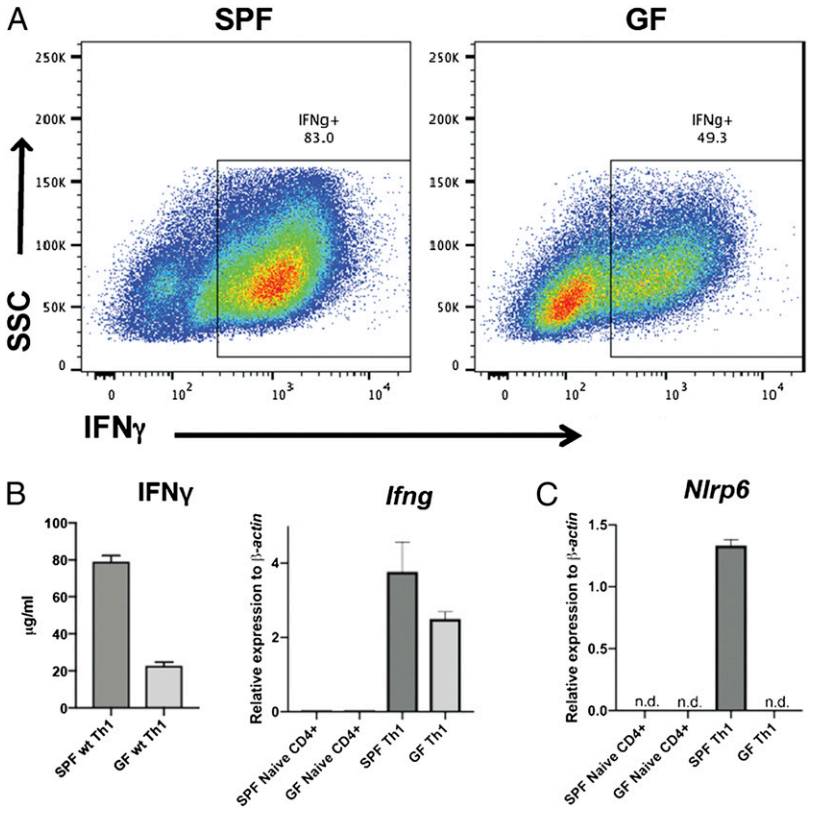

FIGURE 3. Nlrp6 expression in in vitro–differentiated SPF and GF Th1 cells. (**A**) Naive CD4$^+$ T cells from C57BL/6 mice that were kept under SPF or from GF conditions were differentiated into Th1 cells. Percentage of IFN-γ–positive cells were detected by flow cytometry on day 5 of culture. (**B**) Quantification of secreted IFN-γ in the supernatants and *Ifng* transcripts were performed by ELISA and qPCR, respectively. (**C**) Nlrp6 expression in Th1 cells differentiated from naive T cells isolated from SPF or GF animals were measured by qPCR. CD4$^+$ T cells from two GF mice were pooled for Th1 polarization; n.d., not detected.

Th1-differentiation conditions did not induce IFN-γ production by *Tbx21*-deficient T cells (Supplemental Fig. 3A). These results suggest that *Nlrp6* expression is induced in T cells upon their initial phase of Th1 differentiation, and the TBX21 transcription factor is required for induction of *Nlrp6* in Th1 cells.

Decreased IFN-γ production by Nlrp6-deficient Th1 cells

IFN-γ production of *Nlrp6*-deficient Th1 cells were measured by flow cytometry at day 5 of differentiation culture (Fig. 2A). The frequency and number of IFN-γ producing cells were significantly reduced in *Nlrp6*-deficient Th1 cells compared with wt (Fig 2B, 2C). IFN-γ secretion was significantly higher following PMA/ionomycin stimulation of Th1 cells as quantified by ELISA (Fig. 2D). During the differentiation culture, IFN-γ production was measured by flow cytometry, and T cells began to produce IFN-γ after day 3, with lower IFN-γ production by *Nlrp6*-deficient T cells compared with wt (Fig. 2E, 2F). To determine if the decrease in IFN-γ production in *Nlrp6*-deficient T cells depends on the assembling of the inflammasome, naive T cells from *Asc*-deficient mice were differentiated into Th1 cells. *Asc*-deficient Th1 cells expressed similar levels of IFN-γ compared with wt Th1 cells, suggesting that reduced IFN-γ production by *Nlrp6*-deficient Th1 cells is ASC independent (Supplemental Fig. 3B, 3C). Differences in IL-18 concentrations between wt and *Nlrp6*-deficient Th1 cell in supernatants of T cell cultures were not observed (Supplemental Fig. 3D). Furthermore, naive T cells isolated from the spleen of *Nlrp6*-deficient and wt mice were differentiated into Th2, Th17, and Treg cells. Similar frequencies and numbers of IL-13–producing Th2, IL-17A–producing Th17, and Treg cells were observed in wt and *Nlrp6*-deficient T cells (Fig. 2G, 2H).

Nlrp6 is expressed by in vitro–differentiated Th1 cells from SPF but not form GF mice

It has been reported that NLRP6 may influence the composition of the microbiota (12), and the microbiota may also influence the expression of *Nlrp6* by T cells. Naive CD4$^+$ T cells were isolated from spleens of either SPF or GF C57BL/6 wt animals and were differentiated into Th1 cells. IFN-γ producing cells were determined by flow cytometry; IFN-γ secretion in supernatants and cellular *Ifng* transcripts were quantified by ELISA and qPCR, respectively. IFN-γ production in Th1 cells differentiated from naive GF T cells was reduced as determined by flow cytometry, ELISA, and qPCR (Fig. 3A, 3B). Th1 cells differentiated from naive GF T cells did not express *Nlrp6* in contrast to SPF Th1 cells (Fig. 3C).

Caspase-1 is activated in in vitro–differentiated Nlrp6-deficient Th1 cells

Subsequently, to assess whether the decreased number of IFN-γ producing Th1 cells in *Nlrp6*-deficient mice compared with wt could be explained by lower proliferative capacity of T cells or not, a proliferation analysis was performed. T cells were first stained for Ki67, which indicate cells in the active phase of the cell cycle (Fig. 4A). Approximately 40% of the T cells were in the active phase of the cell cycle on day 2 of the culture under Th1 conditions (Fig. 4B), and all cells were in the active phase of the cell cycle on day 5 of culture (Fig. 4B). The difference between *Nlrp6*-deficient and wt Th1 cells was not statistically significant until day 5, when lower number of Ki67$^+$ cells was observed because of the lower number of living cells in *Nlrp6*-deficient cultures (Fig. 4A, 4C). T cells were also labeled with CFSE, and dye dilution was measured by flow cytometry to monitor cell proliferation (Fig. 4D). Th1 cells from both *Nlrp6*-deficient and wt mice underwent five cycles during 3 d of culture. The CFSE dye was diluted out similarly by *Nlrp6*-deficient and wt Th1 cells after 5 d of culture. No difference in proliferation of *Nlrp6*-deficient and wt mice was observed in the CFSE dilution assay. To investigate whether the reduced numbers of IFN-γ producing Th1 cells in *Nlrp6*-deficient mice was associated with cell death or not, annexin/viability assay was performed. T cells were stained with

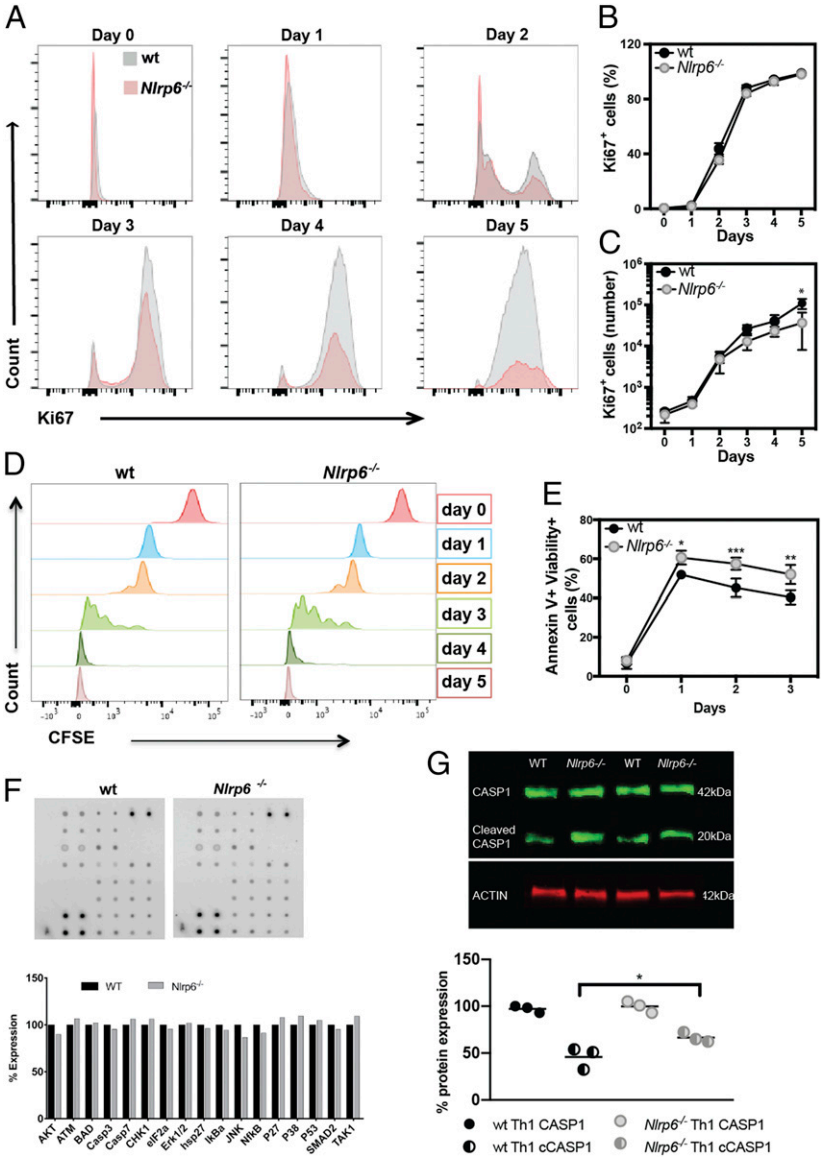

FIGURE 4. T cell proliferation is not influenced by NLRP6. (**A**) Naive CD4$^+$ T cells from wt and *Nlrp6*-deficient mice were differentiated into Th1 cells and stained for Ki67 for flow cytometric analysis at indicated time points. Wt and *Nlrp6*-deficient CD4 T$^+$ cells were shown in gray and red histograms, respectively. (**B**) Percentage of Ki67$^+$ cells and (**C**) number of Ki67$^+$ cells were determined. Mean and SD at indicated time points are shown ($n = 3$ for each group). Statistical significance ($p < 0.05$) was not reached in the Kruskal–Wallis test. (**D**) Naive CD4$^+$ T cells from wt and *Nlrp6*-deficient mice were labeled with CFSE and analyzed by flow cytometry. (**E**) Naive CD4$^+$ T cells were differentiated into Th1 cells, and the percentage of annexin V$^+$/viability$^+$ T cells was determined by flow cytometry at indicated time points; results are presented as mean ± SD ($n = 3$ for all groups). Data were analyzed by Kruskal–Wallis test. (**F**) Isolated proteins from wt and *Nlrp6*-deficient Th1 cells were probed on a membrane-based apoptosis signaling pathway. Internal positive and negative controls were used for array normalization and background noise compensation. Two wt and two *Nlrp6*-deficient Th1 samples were pooled for the assay. (**G**) Caspase1 and cleaved-Caspase1 expression in wt and *Nlrp6*-deficient Th1 cells was measured by western blot. Data were analyzed with Kruskal–Wallis test. *$p < 0.05$, **$p < 0.01$, ***$p < 0.001$.

annexin V at various time points during Th1 differentiation. Increased frequency of annexin V$^+$ viability$^+$ cells were observed in *Nlrp6*-deficient cells compared with wt (Fig. 4E). Because both pyroptotic and apoptotic cells show positive annexin V staining (18, 19), we used an apoptosis signaling pathways array and detection of caspase-1activation by Western blot to investigate the possible presence of apoptotic and pyroptotic pathways in *Nlrp6*-deficient T cells. The used mouse apoptosis signaling pathway protein array detects 17 phosphorylated or cleaved mouse proteins. Phosphorylated or cleaved AKT, ATM, BAD, Casp3, Casp7, CHK1, elF2a, Erk1/2, hsp17, IkBa, JNK, NfkB, p27, p38, p53, SMAD2, and TAK1 did not differ between wt and *Nlrp6*-deficient Th1 cells (Fig. 4F). In contrast, Western blot analysis showed that *Nlrp6* deficiency led to significant activation of caspase-1, indicating that caspase-1–induced T cell death is initiated in *Nlrp6*-deficient T cells (Fig. 4G).

In vivo T cell development is not affected by NLRP6 deficiency

First, *Nlrp6*$^{-/-}$ and wt lymphocytes isolated from the thymus were analyzed for changes in T cell compartment. The frequency and number of CD4 and CD8 single-positive and double-positive cells were not significantly different (Supplemental Fig. 4). *Nlrp6*-deficient and wt CD4 T cells isolated from the spleen, mln, colonic lamina propria (cLP) and small intestine lamina propria (siLP) of littermate mice were stained for IFN-γ and IL-17A for flow cytometric analysis. CD4 T cell frequencies were similar in the spleen and cLP; in contrast, a slight decrease was observed in mln and siLP that did not reach statistical significance (Fig. 5). Intracellular staining of IFN-γ and IL-17A showed no significant difference in frequencies of IFN-γ$^+$, IL-17A$^+$, and IFN-γ/IL-17A double-positive T cells in the spleen, mln, cLP, and siLP (Fig. 5).

Reduced numbers of Nlrp6-deficient T cells compared with wt T cells after cotransfer in Rag2-deficient hosts

Equal numbers of naive wt CD45.1 CD4 CD45RB^{high} and *Nlrp6*-deficient CD45.2 CD4 CD45RB^{high} T cells were transferred in *Rag2*$^{-/-}$ mice, and the differentiation of CD4 T cells in the spleen, mln, and cLP was determined by flow cytometry (Fig. 6A). Two weeks after transfer, CD4 T cells were found in all analyzed organs, with the highest T cell numbers in the cLP (Fig. 6B). Higher frequencies of CD4 T cells derived from wt animals compared with T cells originating from *Nlrp6*-deficient mice were observed in spleen and mln 2 wk after transfer (Fig. 6C). The frequency and number of wt CD4 T cells in the spleen, mln, and cLP were higher in comparison with *Nlrp6*-deficient CD4 T cells 3 wk after transfer (Fig. 6C). Frequency of IFN-γ–producing, but

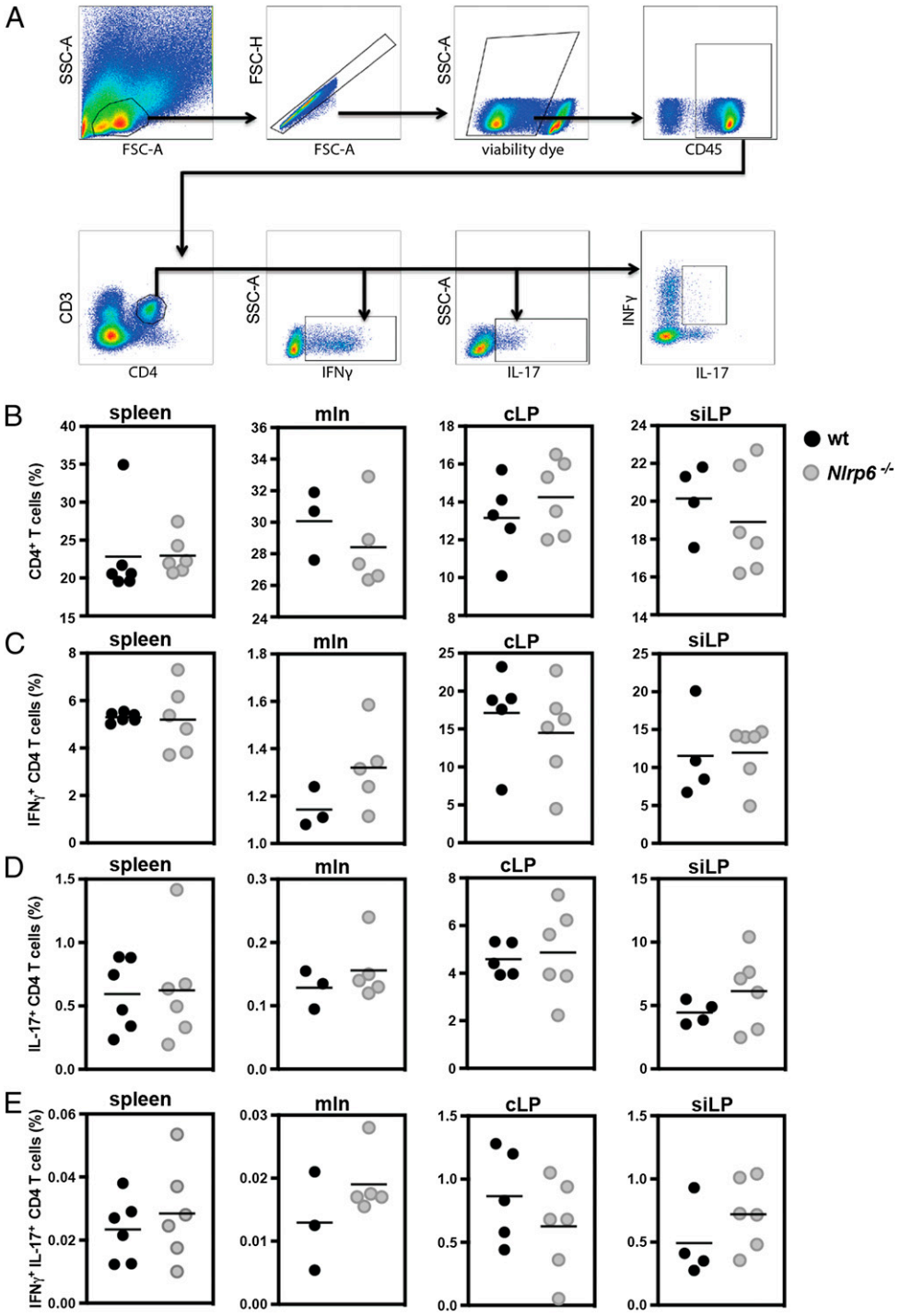

FIGURE 5. Steady-state T cell development is NLRP6 independent. (**A**) Gating strategy for the detection of different T cell subsets in mice. After exclusion of dead cells $CD4^+$ T cells were selected within $CD45^+$ leukocytes. Percentages of IFN-γ^+, IL-$17A^+$, and IFN-γ/IL-17A double-positive T cells were determined. Frequencies of (**B**) $CD4^+$ T cells, (**C**) IFN-γ^+CD4^+ T cells, (**D**) IL-$17A^+CD4$ T^+ cells, and (**E**) IFN-γ/IL-17A double-positive $CD4^+$ T cells from wt and *Nlrp6*-deficient mice were determined in the spleen, mln, cLP, and siLP. Each data point represents an individual animal, and the mean of the results is presented. Statistical significance ($p < 0.05$) was not reached in the Mann–Whitney *U* test.

not of IL-17A– and IFN-γ/IL-17A–producing, CD4 T cells were reduced in *Nlrp6*-deficient T cell population in the mln comparing with wt cells 3 wk after transfer (Fig. 6D).

Enrichment of hallmark signatures in Nlrp6-deficient T cells associated with cell death

CD45.1 wt CD4 T cells and CD45.2 *Nlrp6*-deficient CD4 T cells were sorted from *Rag2*-deficient hosts 3 wk after adoptive T cell cotransfer, RNA was extracted, and the transcriptomes of wt and *Nlrp6*-deficient CD4 T cells were analyzed using RNA sequencing (RNA-seq). A principal component analysis revealed that wt CD4 T cells and *Nlrp6*-deficient CD4 T cells formed two distinct clusters on the first principal component, explaining 29.4% of the variation (Fig. 7A). The influence of the host mice (replicates) was only apparent on the fourth principal component, explaining 11.7% of the variation. One of the most differentially expressed genes was *Nlrp6*, which was highly expressed in *Nlrp6*-deficient animals (data not shown). As the first two exons of *Nlrp6* have

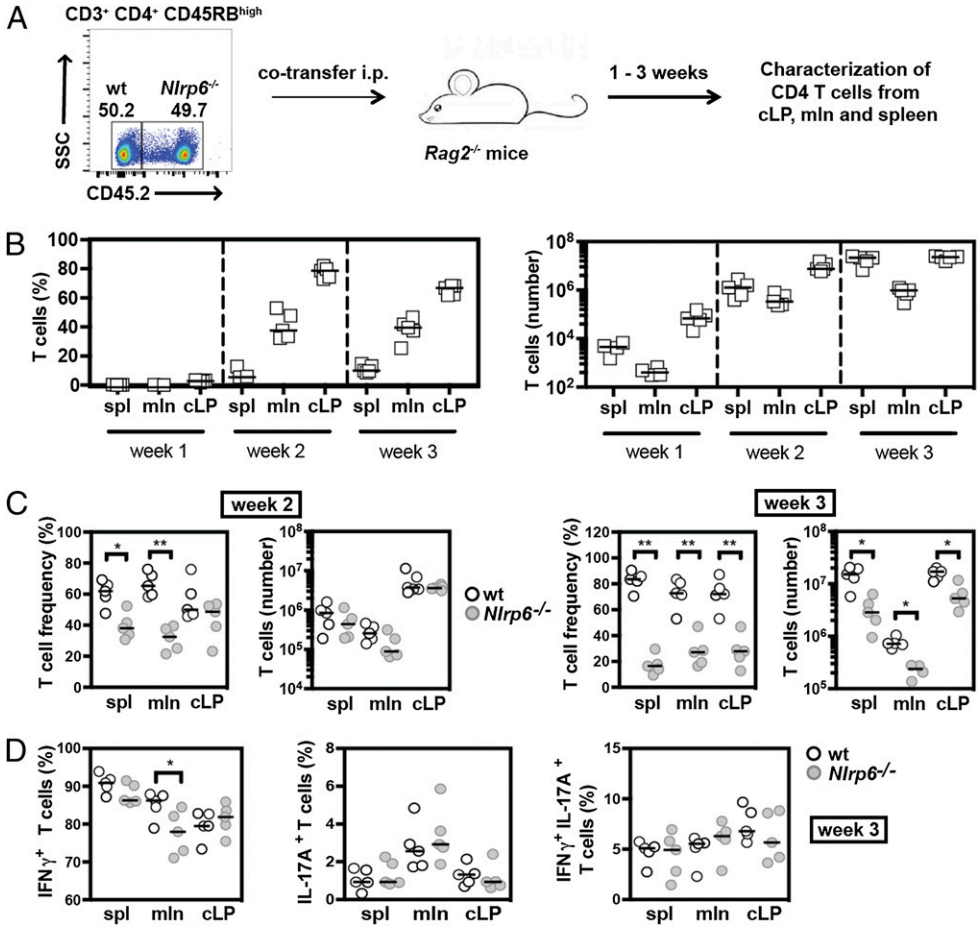

FIGURE 6. Reduced T cell numbers after transfer of *Nlrp6*-deficient T cells. (**A**) Equal numbers of CD45.1$^+$ wt and CD45.2$^+$ *Nlrp6*-deficient CD45RB^{high} T cells were adoptively transferred in *Rag2*-deficient mice, and T cells in reconstituted mice were analyzed 1–3 wk after transfer. (**B**) The percentage and number of CD4$^+$ T cells were analyzed in the spleen (spl), mln, and cLP of *Rag2*-deficient hosts at indicated time points. Each square represents an individual animal; results are presented as median. (**C**) The frequency and number of wt and *Nlrp6*-deficient T cells were analyzed 2- and 3- wk following transfer into *Rag2*-deficient hosts. (**D**) Percentage of IFN-γ$^+$, IL-17A$^+$, and IFN-γ/IL-17A double-positive T cells in *Rag2*-deficient hosts 3 wk after cotransfer of wt and *Nlrp6*-deficient T cells. Each dot represents one individual animal, $n = 5$ for each group, and the median of the results is presented. Data were analyzed with a Mann–Whitney U test. $^*p < 0.05$, $^{**}p < 0.01$.

been replaced by a neomycin cassette, the deletion of *Nlrp6* may result in increased expression of exons 3–8. Therefore, Nlrp6 was not further considered in our analysis. The transcriptional signature of wt CD4 T cells and *Nlrp6*-deficient CD4 T cells is apparent in a heatmap showing the expression of 628 genes downregulated and 923 genes upregulated genes in *Nlrp6*-deficient CD4 T cells compared with wt (Fig. 7B). Because of the high number of differentially expressed genes, we used a gene set enrichment analysis to characterize them. The comparison of the differentially expressed genes to the MSigDB hallmark signatures, revealed that hallmark signatures associated with cell death, such as IFN -γ response, inflammatory response, IL-6 JAK STAT3 signaling, and TNF-α signaling were enriched in *Nlrp6*-deficient compared with wt CD4 T cells (Fig. 7C). Overlap of genes between the individual hallmark collections is presented by heatmap (Fig. 7D). Because reduced numbers of *Nlrp6*-deficient T cells following transfer of T cells in *Rag2*-deficient hosts and enrichment of hallmark signatures associated with cell death in RNA-seq experiments was observed, gene families associated with cell death, such as Toll, IL, IFN, Traf, Ripk, Nlr, Cytochrome, Granzyme, Fadd and Caspase, were tested for enrichment of differentially expressed genes (Table II). Upregulated ILs in *Nlrp6*-deficient T cells included *Il-1β*, *Il-6*, and their receptors (Fig. 7E). Furthermore, *Tlr6*, *Tlr4*, *Tlr9*, and *Tlr2* were upregulated in *Nlrp6*-deficient cells (Fig. 7F). Inflammatory-associated caspase recruitment domain (CARD), such as Card11, were upregulated, whereas the caspases 3 and 7 were downregulated (Fig. 7G).

Nlrp6 deficiency in CD4 T cells decreased T cells survival in Rag2$^{-/-}$ hosts

To confirm increased cell death in *Nlrp6*-deficient T cells, annexin V and fixable viability dye staining were used. The frequency and number of annexin V$^+$ T cells were determined 2 and 3 wk following cotransfer of wt and *Nlrp6*-deficient CD4$^+$ T cells into *Rag2*$^{-/-}$ hosts. Frequency of annexin V$^+$/fixable viability dye-negative cells, but not of annexin V$^+$/fixable viability dye-positive (dead) cells, were higher in *Nlrp6*-deficient CD4$^+$ T cells compared with wt 2 wk after cotransfer (Fig. 8A). Increased frequency of annexin V$^+$/fixable viability dye-positive (dead) cells among *Nlrp6*-deficient T cells was noted 3 wk after cotransfer (Fig. 8B). Differences in the frequency of annexin V$^+$/fixable viability dye-negative cells disappeared 3 wk after cotransfer (Fig. 8B), indicating a window of 2–3 wk after cell transfer, in which *Nlrp6*-deficient CD4$^+$ T cells undergo cell death. *Nlrp6*-deficient CD4$^+$ T cells and C57BL/6 wt T cells were then separately transferred in different *Rag2*$^{-/-}$ hosts, and the course of transfer colitis was monitored by measuring the body weight and determining disease scores. Both *Rag2*$^{-/-}$ hosts receiving *Nlrp6*-deficient T cells and wt T cells had reduced body weight gain

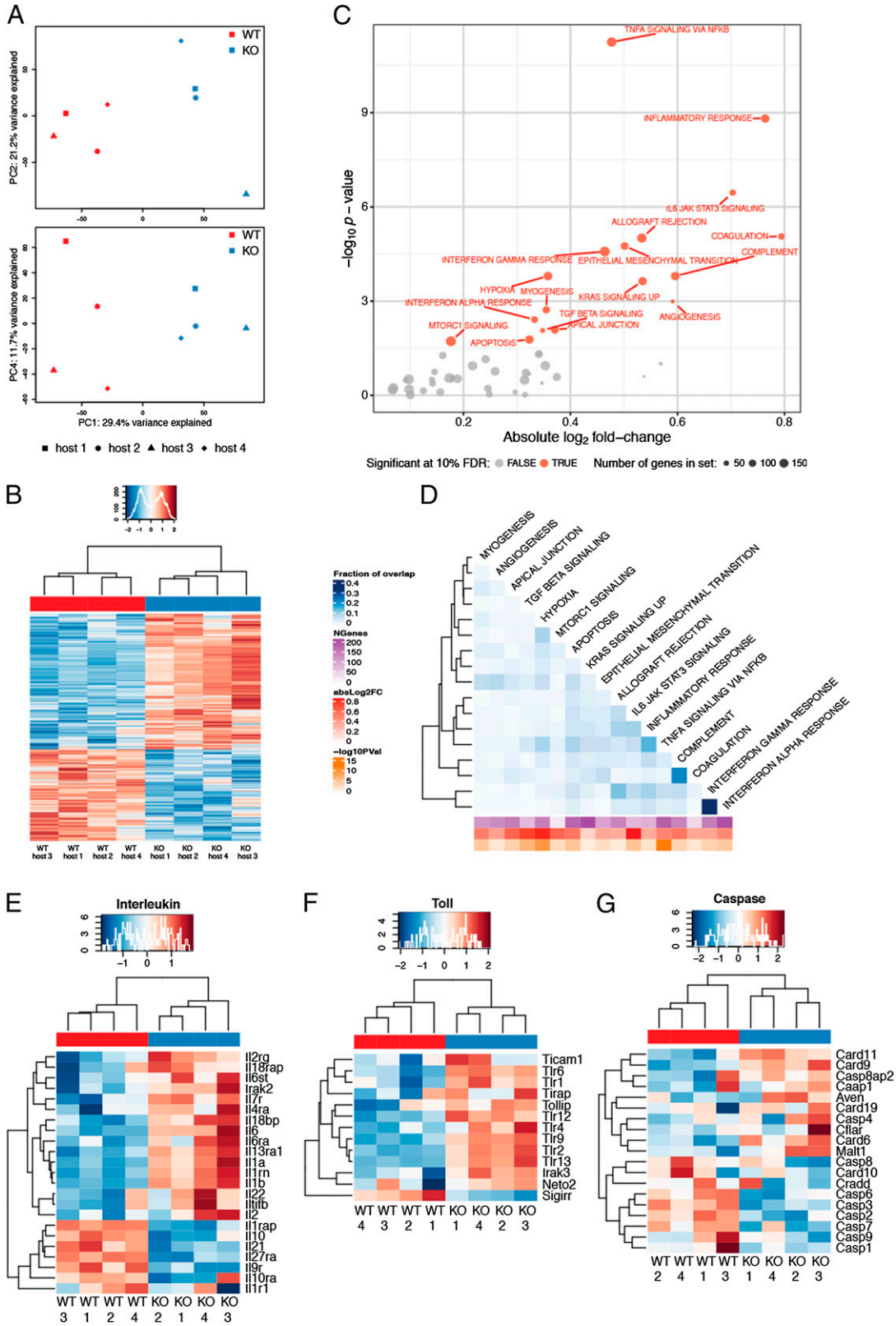

FIGURE 7. Cell death signatures are enriched in *Nlrp6*-deficient T cells *Rag2*-deficient hosts were reconstituted with equal numbers of wt and *Nlrp6*-deficient CD4$^+$ T cells. Following the reconstitution period (3 wk), CD4$^+$ T cells were isolated from the cLP and analyzed by RNA-seq. (**A**) Principle component analysis PC1 versus PC2 and PC1 versus PC4 of wt and *Nlrp6*-deficient CD4$^+$ T cells samples. (**B**) Heatmap of all differentially expressed genes between wt and *Nlrp6*-deficient CD4$^+$ T cells (FDR 5%). (**C**) Significantly enriched MSigDB hallmark signatures in *Nlrp6*-deficient T cells. FDR was defined to be significant at 10%; circle size indicates the number of enriched genes. (**D**) Overlap of genes between hallmark signatures is indicated by the color intensity on the heatmap. Custom selected heatmaps indicate differentially expressed genes among (**E**) ILs, (**F**) Tolls, and (**G**) Caspases between wt and *Nlrp6*-deficient CD4$^+$ T cells.

Table II. Differential regulated genes in RNA-seq analysis of wt and *Nlrp6*-deficient T cells

	No. of Genes	Direction	absLog2FC	*p* Values	FDR
Toll	13	Up	1.2	4.6×10^{-9}	4.6×10^{-8}
IL	23	Up	1.2	2.0×10^{-3}	0.01
IFN	51	Up	0.33	4.4×10^{-3}	0.015
Traf	16	Up	0.45	0.13	0.33
Ripk	4	Up	0.15	0.28	0.56
Nlr	13	Up	0.35	0.38	0.63
Cytochromes	64	Up	0.23	0.64	0.90
Granzyme	5	Down	0.53	0.72	0.90
Fadd	2	Up	0.063	0.97	1
Caspase	19	Up	0.24	1	1

absLog2FC, absolute Log2 fold change; Down, downregulated in *Nlrp6*-deficient T cell; Up, upregulated in *Nlrp6*-deficient T cell.

compared with nontransplanted *Rag2*$^{-/-}$ animals (Fig. 8C). Clinical signs of colitis and differences in body weight change initially occurred at day 12 after transfer of wt CD4$^+$ T cells, whereas clinical colitis signs appeared between 12 and 19 d after transfer of *Nlrp6*-deficient CD4$^+$ T cells into *Rag2*$^{-/-}$ hosts (Fig. 8C, 8D). Histological colitis scores and images showed no difference at day 28 (Fig. 8E, 8F). Annexin V staining analysis showed no difference in dead and annexin V$^+$ cells between wt and *Nlrp6*-deficient CD4$^+$ T cells 4 wk following the transfer (Fig. 8G).

Discussion

The generation of effector T cells depends on microbial-derived factors and cytokines, which is required for host defense to extracellular and intracellular pathogens (27). In particular, high numbers of effector and regulatory T cells in the intestine is required for the maintenance of the balance between the host and microbiota (28). During an immune response against pathogens, the stimulation of T cells with Ags lead to their proliferation as well as to the generation of effector cells required for the clearance of pathogens. Upon elimination of the pathogen, activated T cells have to be systematically removed, because otherwise, they may induce autoimmune diseases and inflammatory bowel disease (27). T cells that are restimulated with Ag after the shutdown of the immune response are removed by activation-induced cell death (29). Conversely, activated T cells that are not restimulated die by activated cell autonomous death (29). In this study, we demonstrate that Th1 cells express *Nlrp6*, which facilitates their survival.

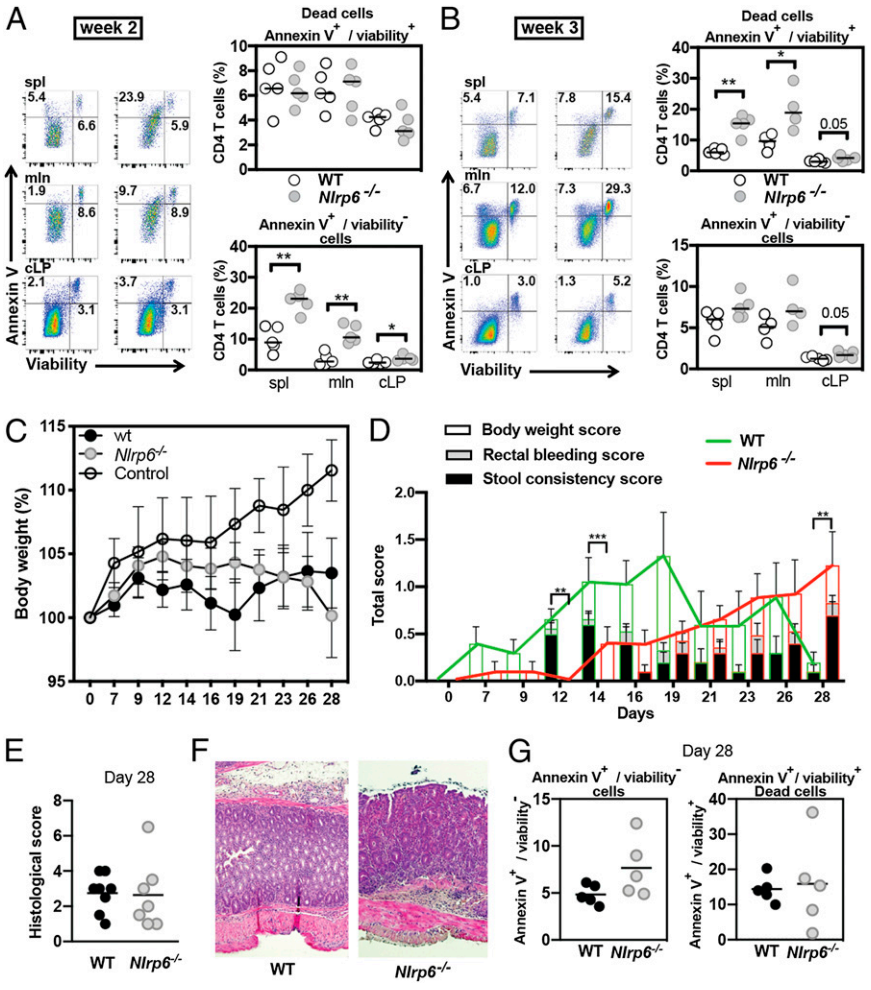

FIGURE 8. Increased cell death in *Nlrp6*-deficient T cells. CD4$^+$ T cells were isolated from the spleen (spl), mln, and cLP 2 or 3 wk after they were transplanted into *Rag2*-deficient mice. T cells were stained for annexin V and viability dye. Values in dot plots indicate the percentage of cells in respective quadrants. Annexin V$^+$/viability$^+$ T cells and annexin V$^+$/viability$^-$ T cells are presented in scatter plots (**A**) after 2 wk and (**B**) after 3 wk following the cotransfer. Each animal is represented by a data point, and the median is shown by horizontal line. Data were analyzed with Mann–Whitney *U* test. Wt or *Nlrp6*-deficient naive T cells were separately transferred into *Rag2*-deficient hosts. (**C**) Percentage body weight change and (**D**) disease activity scores (body weight loss, stool consistency, and rectal bleeding) during 4 wk after transfer. Data are mean ± SEM (n = 8). Statistic for stool consistency score was calculated using multiple Mann–Whitney tests. (**E**) Histological score analysis and (**F**) images of *Rag2*-deficient hosts reconstituted with wt or *Nlrp6*-deficient CD4$^+$ T cells, (**G**) annexin V$^+$, and dead cell populations 28 d after transfer as quantifies by annexin V and viability staining. Each animal is represented by a data point, and the median is shown by horizontal line (A, B, E, and G). *p < 0.05, **p < 0.01, ***p < 0.001.

Our results suggest that the expression of *Nlrp6* by Th1 cells depends on the presence of an intact microbiota, because the differentiation of naive T cells from GF mice into Th1 cells did not induce *Nlrp6* expression. In vitro–differentiated Th1 cells from GF mice are characterized by reduced IFN-γ production any may thereby prevent *Nlrp6* expression in T cell cultures in which no bacteria are present. As binding sites for TBX21 in the promoter regions of *Nlrp6* were identified, and *Nlrp6* expression was not observed in *Tbx21*-deficient Th1 cells, we believe that TBX21 promotes the expression of *Nlrp6* in T cells. We cannot rule out an influence of microbial-derived spermidine or taurine, which have been suggested as potential ligands of NLRP6 in the in vitro cultures. Although it has been reported that spermidine or taurine may be present in the FCS supplemented to the culture medium (7), they may rather cause intrinsic effects on T cells than mediating microbial-derived signal on T cells through NLRP6. To avoid the influence of possible different microbiotas in C57BL/6 wt and *Nlrp6*-deficient mice, T cells from C57BL/6 wt and *Nlrp6*-deficient mice were cotransferred into the same *Rag2*$^{-/-}$ hosts. Cotransferred T cells are exposed to the same microbiota or microbial-derived products to minimize effects of different microbiotas present in C57BL/6 wt and *Nlrp6*-deficient mice as much as possible.

NLRP6 has the ability to assemble with ASC to form the inflammasome (30); in contrast, reduced IFN-γ production was observed in *Nlrp6*-deficient, but not *Asc*-deficient, Th1 cells in vitro, suggesting that the reduced IFN-γ production in *Nlrp6*-deficient Th1 cells is ASC/inflammasome independent. Consistently, activation of the TCR or stimulation of T cells with ATP induces the production of pro–IL-1β, which is cleaved by caspase-1 in an ASC-dependent manner. IL-1β acts in an autocrine fashion on Th17 cells expressing IL-1R to mediate survival, but not on Th1 cells that lack IL-1R (31). Although reduced Th1 and Th17 cells have been reported in infected *Asc*-deficient animals (32), IFN-γ production by in vitro–differentiated and *Asc*-deficient Th1 cells was not impaired (33).

Furthermore, increased cell death was observed in *Nlrp6*-deficient T cells. RNA-seq revealed significant upregulation of hallmark signatures associated with cell death. Increased caspase-1 activation was observed in *Nlrp6*-deficient T cells by biochemical means, suggesting caspase-1 dependent cell death (pyroptosis) in absence of NLRP6, which is in contrast to findings that have demonstrated caspase-1 activation by the NLRP6 inflammasome. Different cells used for these studies may explain the different findings as mainly macrophages and IEC, but not T cells, have previously been studied (5, 7, 8, 12). Second, experiments with *Asc*-deficient mice suggested that the effects of NLPR6 on T cells are ASC/inflammasome independent. In conclusion, CD4^{+} T cells express *Nlrp6*, which facilitates their survival in vitro and after transfer in *Rag2*-deficient hosts. Future studies are needed to further elucidate the pathways by which NLRP6 facilitates survival of Th1 cells. Our findings indicate that the expression of NLRP6 by T cells is influenced by an intact microbiota, and the survival of T cells is controlled by NLRP6 in an intrinsic manner.

Acknowledgments

We thank Philippe Demougin for assistance with RNA-seq and Julien Roux for bioinformatics analysis of the RNA-seq data. The Takeda Oncology company provided the *Nlrp6*-deficient animals, which were originally generated at Millenium Pharmaceuticals. For the RNA-seq analysis, calculations were performed at sciCORE (http://scicore.unibas.ch/) scientific computing center at University of Basel.

Disclosures

The authors have no financial conflicts of interest.

References

1. Levy, M., H. Shapiro, C. A. Thaiss, and E. Elinav. 2017. NLRP6: a multifaceted innate immune sensor. *Trends Immunol.* 38: 248–260.
2. Strowig, T., J. Henao-Mejia, E. Elinav, and R. Flavell. 2012. Inflammasomes in health and disease. *Nature* 481: 278–286.
3. Grenier, J. M., L. Wang, G. A. Manji, W. J. Huang, A. Al-Garawi, R. Kelly, A. Carlson, S. Merriam, J. M. Lora, M. Briskin, et al. 2002. Functional screening of five PYPAF family members identifies PYPAF5 as a novel regulator of NF-kappaB and caspase-1. *FEBS Lett.* 530: 73–78.
4. Kayagaki, N., I. B. Stowe, B. L. Lee, K. O'Rourke, K. Anderson, S. Warming, T. Cuellar, B. Haley, M. Roose-Girma, Q. T. Phung, et al. 2015. Caspase-11 cleaves gasdermin D for non-canonical inflammasome signalling. *Nature* 526: 666–671.
5. Anand, P. K., R. K. Malireddi, J. R. Lukens, P. Vogel, J. Bertin, M. Lamkanfi, and T. D. Kanneganti. 2012. NLRP6 negatively regulates innate immunity and host defence against bacterial pathogens. *Nature* 488: 389–393.
6. Wang, P., S. Zhu, L. Yang, S. Cui, W. Pan, R. Jackson, Y. Zheng, A. Rongvaux, Q. Sun, G. Yang, et al. 2015. Nlrp6 regulates intestinal antiviral innate immunity. *Science* 350: 826–830.
7. Levy, M., C. A. Thaiss, D. Zeevi, L. Dohnalová, G. Zilberman-Schapira, J. A. Mahdi, E. David, A. Savidor, T. Korem, Y. Herzig, et al. 2015. Microbiota-modulated metabolites shape the intestinal microenvironment by regulating NLRP6 inflammasome signaling. *Cell* 163: 1428–1443.
8. Hara, H., S. S. Seregin, D. Yang, K. Fukase, M. Chamaillard, E. S. Alnemri, N. Inohara, G. Y. Chen, and G. Nunez. 2018. The NLRP6 inflammasome recognizes lipoteichoic acid and regulates gram-positive pathogen infection. *Cell* 175: 1651–1664.e14.
9. Chen, G. Y., M. Liu, F. Wang, J. Bertin, and G. Núñez. 2011. A functional role for Nlrp6 in intestinal inflammation and tumorigenesis. *J. Immunol.* 186: 7187–7194.
10. Wlodarska, M., C. A. Thaiss, R. Nowarski, J. Henao-Mejia, J. P. Zhang, E. M. Brown, G. Frankel, M. Levy, M. N. Katz, W. M. Philbrick, et al. 2014. NLRP6 inflammasome orchestrates the colonic host-microbial interface by regulating goblet cell mucus secretion. *Cell* 156: 1045–1059.
11. Birchenough, G. M., E. E. Nyström, M. E. Johansson, and G. C. Hansson. 2016. A sentinel goblet cell guards the colonic crypt by triggering Nlrp6-dependent Muc2 secretion. *Science* 352: 1535–1542.
12. Elinav, E., T. Strowig, A. L. Kau, J. Henao-Mejia, C. A. Thaiss, C. J. Booth, D. R. Peaper, J. Bertin, S. C. Eisenbarth, J. I. Gordon, and R. A. Flavell. 2011. NLRP6 inflammasome regulates colonic microbial ecology and risk for colitis. *Cell* 145: 745–757.
13. Normand, S., A. Delanoye-Crespin, A. Bressenot, L. Huot, T. Grandjean, L. Peyrin-Biroulet, Y. Lemoine, D. Hot, and M. Chamaillard. 2011. Nod-like receptor pyrin domain-containing protein 6 (NLRP6) controls epithelial self-renewal and colorectal carcinogenesis upon injury. *Proc. Natl. Acad. Sci. USA* 108: 9601–9606.
14. Seregin, S. S., N. Golovchenko, B. Schaf, J. Chen, N. A. Pudlo, J. Mitchell, N. T. Baxter, L. Zhao, P. D. Schloss, E. C. Martens, et al. 2017. NLRP6 protects Il10$^{-/-}$ mice from colitis by limiting colonization of akkermansia muciniphila. [Published erratum appears in 2017 *Cell Rep.* 19: 2174.] *Cell Rep.* 19: 733–745.
15. Mamantopoulos, M., F. Ronchi, F. Van Hauwermeiren, S. Vieira-Silva, B. Yilmaz, L. Martens, Y. Saeys, S. K. Drexler, A. S. Yazdi, J. Raes, M. Lamkanfi, K. D. McCoy, and A. Wullaert. 2017. Nlrp6- and ASC-dependent inflammasomes do not shape the commensal gut microbiota composition. *Immunity* 47: 339–348.e4.
16. Lemire, P., S. J. Robertson, H. Maughan, I. Tattoli, C. J. Streutker, J. M. Platnich, D. A. Muruve, D. J. Philpott, and S. E. Girardin. 2017. The NLR protein NLRP6 does not impact gut microbiota composition. *Cell Rep.* 21: 3653–3661.
17. Gálvez, E. J. C., A. Iljazovic, A. Gronow, R. Flavell, and T. Strowig. 2017. Shaping of intestinal microbiota in Nlrp6- and rag2-deficient mice depends on community structure. *Cell Rep.* 21: 3914–3926.
18. Man, S. M., R. Karki, and T. D. Kanneganti. 2017. Molecular mechanisms and functions of pyroptosis, inflammatory caspases and inflammasomes in infectious diseases. *Immunol. Rev.* 277: 61–75.
19. Miao, E. A., J. V. Rajan, and A. Aderem. 2011. Caspase-1-induced pyroptotic cell death. *Immunol. Rev.* 243: 206–214.
20. Dobin, A., C. A. Davis, F. Schlesinger, J. Drenkow, C. Zaleski, S. Jha, P. Batut, M. Chaisson, and T. R. Gingeras. 2013. STAR: ultrafast universal RNA-seq aligner. *Bioinformatics* 29: 15–21.
21. Gaidatzis, D., A. Lerch, F. Hahne, and M. B. Stadler. 2015. QuasR: quantification and annotation of short reads in R. *Bioinformatics* 31: 1130–1132.
22. Robinson, M. D., D. J. McCarthy, and G. K. Smyth. 2010. edgeR: a Bioconductor package for differential expression analysis of digital gene expression data. *Bioinformatics* 26: 139–140.
23. Robinson, M. D., and A. Oshlack. 2010. A scaling normalization method for differential expression analysis of RNA-seq data. *Genome Biol.* 11: R25.
24. Wu, D., and G. K. Smyth. 2012. Camera: a competitive gene set test accounting for inter-gene correlation. *Nucleic Acids Res.* 40: e133.
25. Subramanian, A., P. Tamayo, V. K. Mootha, S. Mukherjee, B. L. Ebert, M. A. Gillette, A. Paulovich, S. L. Pomeroy, T. R. Golub, E. S. Lander, and J. P. Mesirov. 2005. Gene set enrichment analysis: a knowledge-based approach for interpreting genome-wide expression profiles. *Proc. Natl. Acad. Sci. USA* 102: 15545–15550.

26. Liberzon, A., C. Birger, H. Thorvaldsdóttir, M. Ghandi, J. P. Mesirov, and P. Tamayo. 2015. The Molecular Signatures Database (MSigDB) hallmark gene set collection. *Cell Syst.* 1: 417–425.
27. Grossman, Z., and W. E. Paul. 2015. Dynamic tuning of lymphocytes: physiological basis, mechanisms, and function. *Annu. Rev. Immunol.* 33: 677–713.
28. Honda, K., and D. R. Littman. 2016. The microbiota in adaptive immune homeostasis and disease. *Nature* 535: 75–84.
29. Brenner, D., P. H. Krammer, and R. Arnold. 2008. Concepts of activated T cell death. *Crit. Rev. Oncol. Hematol.* 66: 52–64.
30. Shen, C., A. Lu, W. J. Xie, J. Ruan, R. Negro, E. H. Egelman, T. M. Fu, and H. Wu. 2019. Molecular mechanism for NLRP6 inflammasome assembly and activation. *Proc. Natl. Acad. Sci. USA* 116: 2052–2057.
31. Martin, B. N., C. Wang, C. J. Zhang, Z. Kang, M. F. Gulen, J. A. Zepp, J. Zhao, G. Bian, J. S. Do, B. Min, et al. 2016. T cell-intrinsic ASC critically promotes T(H)17-mediated experimental autoimmune encephalomyelitis. *Nat. Immunol.* 17: 583–592.
32. van de Veerdonk, F. L., L. A. Joosten, P. J. Shaw, S. P. Smeekens, R. K. Malireddi, J. W. van der Meer, B. J. Kullberg, M. G. Netea, and T. D. Kanneganti. 2011. The inflammasome drives protective Th1 and Th17 cellular responses in disseminated candidiasis. *Eur. J. Immunol.* 41: 2260–2268.
33. Bruchard, M., C. Rebé, V. Derangère, D. Togbé, B. Ryffel, R. Boidot, E. Humblin, A. Hamman, F. Chalmin, H. Berger, et al. 2015. The receptor NLRP3 is a transcriptional regulator of TH2 differentiation. [Published erratum appears in 2015 *Nat. Immunol.* 16: 1292.] *Nat. Immunol.* 16: 859–870.

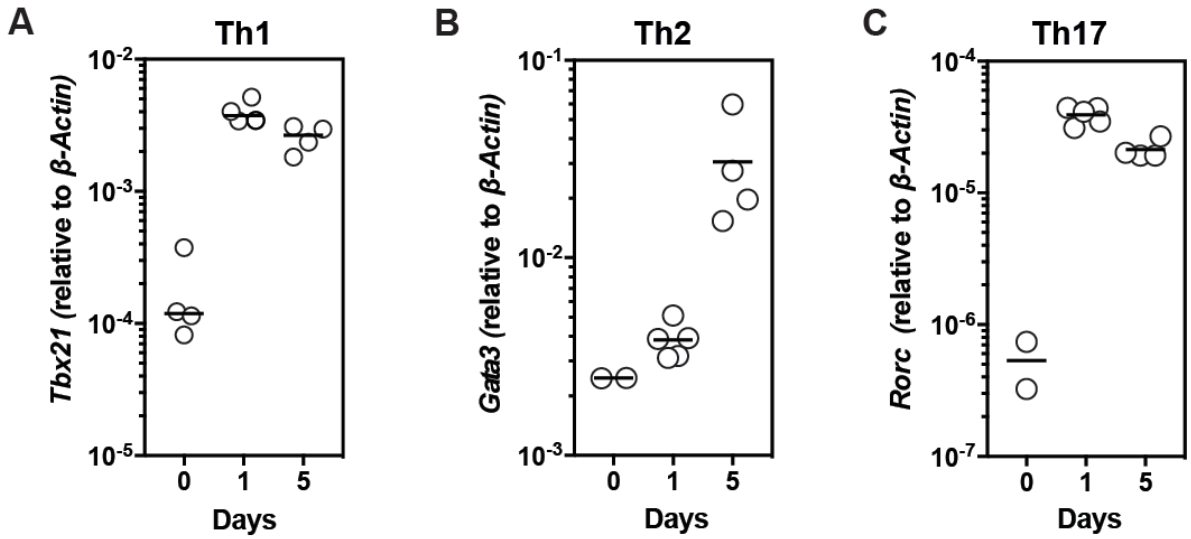

Suppl. figure 1. *Tbx21*, Gata3 and *Rorc* expression by differentiated Th1, Th2 and Th17 cells.

(A) *Tbx21* expression by naïve T cells and differentiated Th1 cells, **(B)** *Gata3* expression by differentiated Th2 cells and **(C)** *Rorc* expression by differentiated Th17 cells at indicated time points during *in vitro* differentiation. Each dot indicates one individual animal; results are shown as median.

A

Mus Musculus Nlrp6 promoter

-1000 tactcgagaccagcttggctttgtatttcttcccttcttccttttttatgtagacgtatgtgttttacacacacacacacacacacacacacacacctg

-900 tataagagttggatatcctgaagctgaagtcataggtggttgatagctacttcatgtgggatcaggaaaccagagtcagtctctttgtgagagacagata

-800 accctaagtgttatctatctctccagcctccctctatcactatcaccttgaaacatttgatatttgagagcacggtggcacgcattccacagattgggtg

-700 tggaggtcagaggacaactttgtggagttcttctctttccacttttctgtgggttccagagttagaactcgagttgtcaggcaagcacctttaccctata

-600 aaccatctcactggccctggcctcacattttctaccttcaataatgatgacaaggagacaaagaagacttgttttccagaatttttataaaaataaataaac

STAT1

-500 acatccatgcctctgtgaactgtgtcttcatggactttatttagtctacgacaaacagtcacttaaatacaacattaacttagccatgtggaggtgtgca

-400 cacgtgcctttacacacgtccgtgccagccacacagtgaaactccatatccctgcagtcacttgcagggcctagggtcagaaacatccgatctctgccct

-300 agagctgggtgtgggaggattaactgactgcagagctgaggacctggttctttttctctctccacccttatccctgcccacaggcccctgccctcttgat

-200 tttcacgccttgtgtgcaaaatttaaagcaccttaaggccatttctgaagacctggttgtgagtcagctatttaatctgaaccacctcacagctgcatag

Eomes

-100 gatgccacacccaggaggaggagtattgatagaataaaatagaagaaaaccaaaggtcgcagtccagcacatatatgatgttacaacccgtgcttaactt

Tbx21 (Tbet)

0 GGGAGCCTCTTGACTGTCAGCAAGAGTCCAGCTGAGCCAGAATGAACAAGACTGAGAAACACCCTCACACCCAGAATGAGACCAGTTTAGCCCAGAAAGG

Eomes STAT5B

TSS

100 ATCACCTCTGCTCCCAGCTTCTGCATCTGAGAGTTAGATCCTGAGATAAGACTCCATGGATGCCGCTGGAGCCTCCTGCTCCAGGTGAGTGTGGTTTCCA

B

Homo sapiens Nlrp6 promoter

-1000 taggcagagcagccccaaaggctgctggttgcccatttttatggttatttcttgattatatgctaaacgaggagtggattattcatgagttttccaggag

STAT1

-900 agtggtggcaattctcagaactgaggttcctcccctttagaccatatagggtaacttcctgactttgccatggcatttataaactgtcatcgtgttg

STAT5B

-800 gtgggagtgtctttagtgtgctaatgtactgtaactagagtaatgagctgtgaggatgaccagaggtcactctcattgccatcttggttctggtggttt

-700 tgggccagcttctttacaccattatcagcaaggcctttatgacctgtatcttgtgtcaacctcctgtctcatcctgtgacttagaatgtctaccctcctg

STAT5A

-600 ggaatgcagcccagtaggtctcagccttattttacccagcacctctcatttccacatattaacccccccgttccacacactctcacatttggtcccaggg

-500 gtctcgaacacccctgacgtccagcctctgcccgccagctgttcaggtcgggtggggaggctgcagtgcagacccctgcccggcgtctccctggagactg

-400 ccttccctcccatatatggtgcgtgctgctggctgtccccccctgttcctctacctggaagtcttttcctcacccctgccttcagagtctaacctctcccc

STAT1

-300 aggcctcagctgaaggcctggctctgagccagccacctccttcacacaacccaccttgctctgaagctgcctgctcacagccatgccccgatgccacacc

Tbx21 (Tbet)

-200 cagggttcttggggaacattaatgggataaaggagtaagaaaatcaaaggtcaccaaacggagcccttaaagggcaatgctctgcgtgtgccacggtgc

-100 ccaacagcatctcgtgccagctgagctgcggtgtgtggacccggggaatggaccgggctggacaacctctaagacttggctccagctcagcctgtgaagg

0 AATCACCTCTCTGATCCCCACCTCTGCCCCGGAGTGCTAGACCCAGGGAGGAAGAGACCCCATGGACCAGCCAGAGGCCCCCTGCTCCAGGTGAGTGCTGG

TSS

C

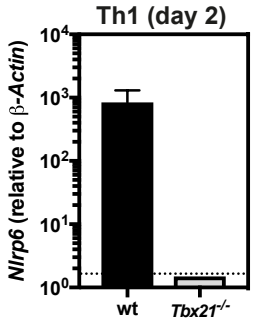

Suppl. figure 2. Genomic regions upstream of *Nlrp6* contains TBX21 binding sites.
(A) Mouse and **(B)** human NLRP6 promoter regions 1000 bp upstream of the indicated transcription starting sites (TSS). Potential STAT1, EOMES, TBX21, STAT5B bindings sites are indicated. **(C)** *Nlrp6* expression by wt and *Tbx21*-deficient $CD4^+$ T cells (n=2) differentiated into Th1 cells for 2 days. Dotted line represents detection limit.

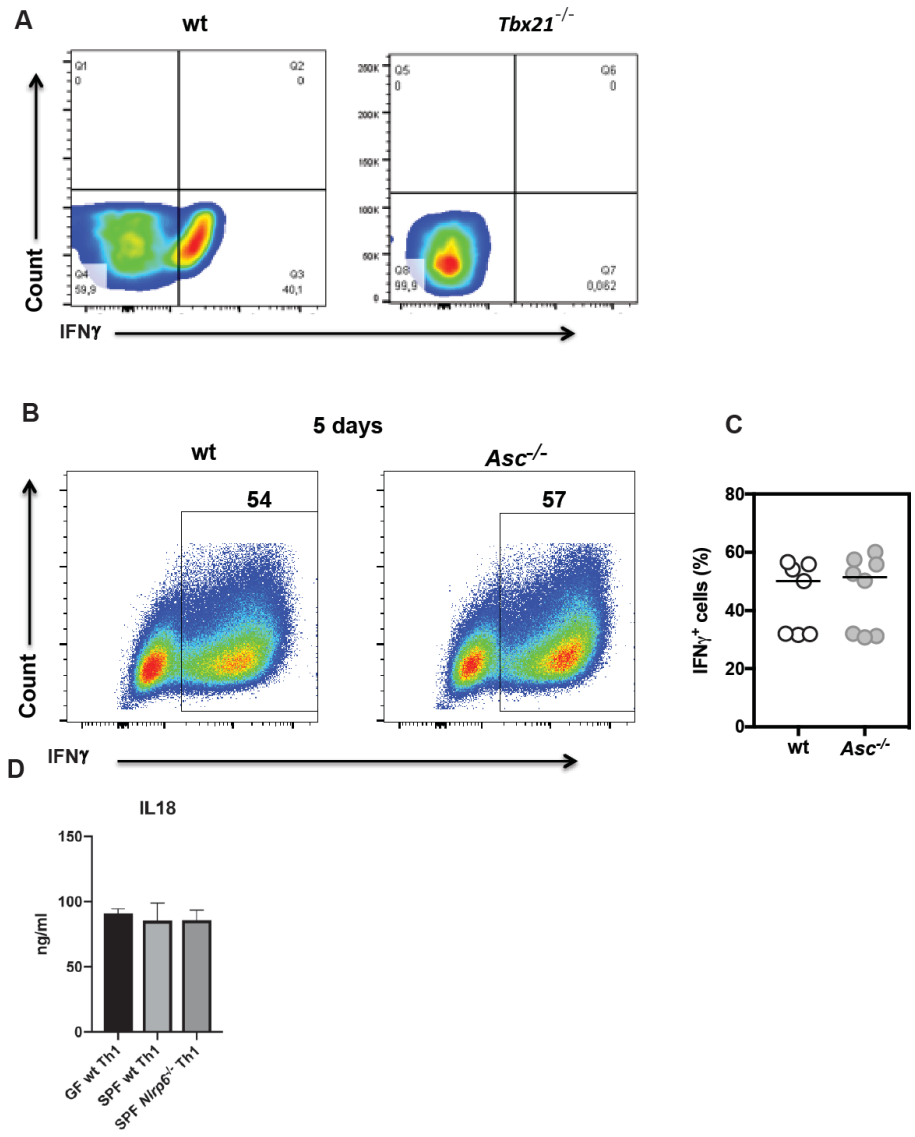

Suppl. figure 3. ASC does not influence Th1 differentiation.

Naïve CD4 T cells from wt, *Tbx21*- and *Asc*-deficient mice were differentiated into Th1 cells for 5 days. (**A**) Numbers in dot blots indicate the percentage of IFNγ producing T cells after differentiation of naïve wt and *Tbx21*-deficient mice under Th1 polarization conditions. **(B)** Numbers indicate the percentage of IFNγ producing T cells in cultures with wt or *Asc*-deficient T cells. **(C)** Results are presented as scatter plots, and the median is shown. Each dot indicates an individual animal. (**D**) IL-18 concentration in supernatants of differentiated naïve CD4 T cells from germ-free (GF) wt mice, standard pathogen free (SPF) wt mice and SPF *Nlrp6*-deficient mice. Supernatants from $CD4^+$ T cell cultures pooled from two GF mice were used; n.d., not detected.

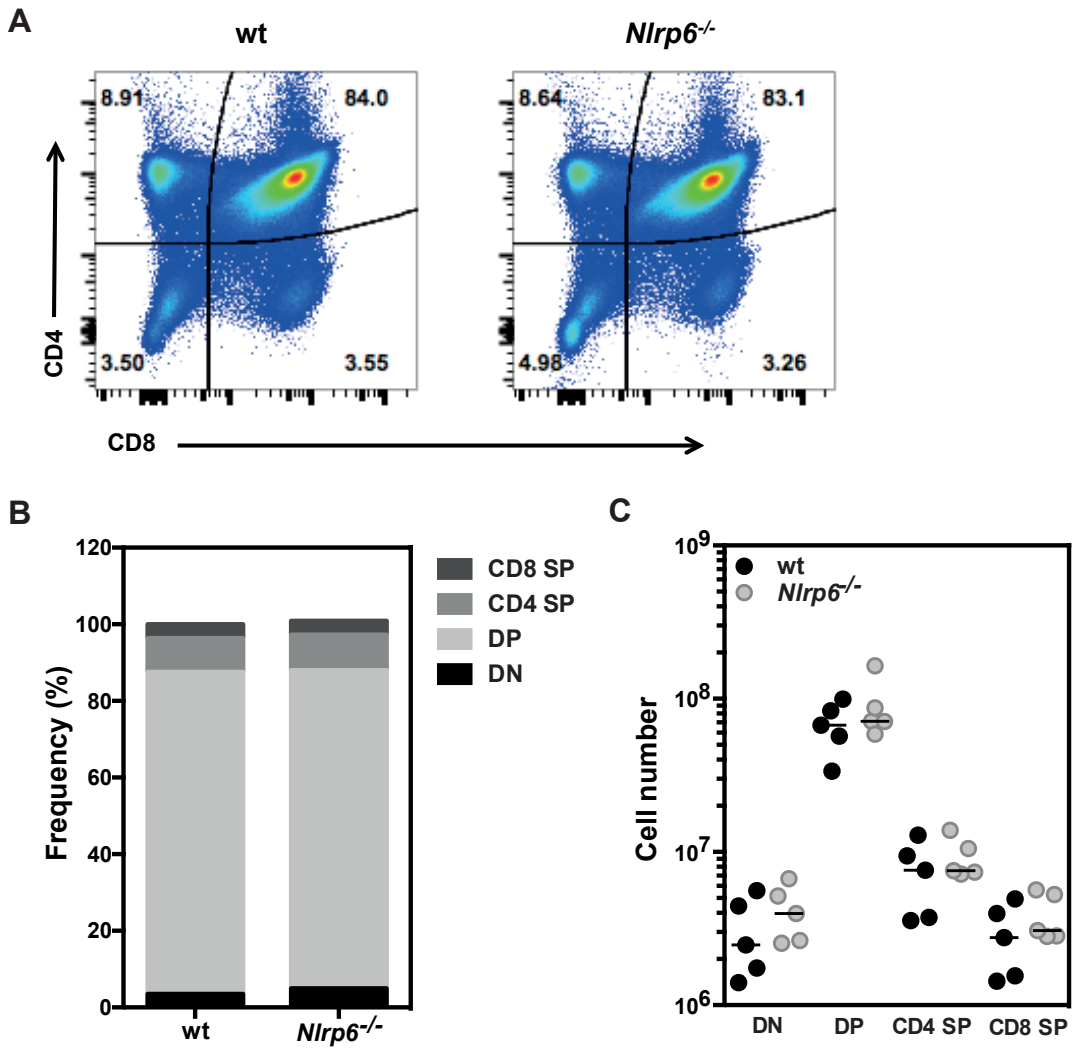

Suppl. figure 4. Steady-state CD4$^+$ T cell development is not influenced by NLRP6.

Lymphocytes were isolated from the thymus of wt and *Nlrp6*-deficient mice and analyzed for CD4 and CD8 expression by flow cytometry. (**A**) CD4/CD8 dot plots of indicated mouse lines were generated by gating on living CD45$^+$ cells. Numbers in dot plots indicate the percentage of cells in the respective quadrants. (**B**) Frequency and (**C**) numbers of CD8 or CD4 single positive (SP), CD4/CD8 double-negative (DN) and CD4/CD8 double-positive (DP). Each dot of the scatter plot represents one individual mouse with the median indicated for each group.